Simultaneous Ground-based and In Situ Swarm Observations of Equatorial F-region Irregularities over Jicamarca

by Aol et al.

Dear Dr. Keisuke Hosokawa,

Thank you for your letter. As authors of the manuscript angeo-2019-153, we thank the referees for their constructive suggestions and comments. In enhancing the quality of the paper, all the remarks we received on this research were taken into consideration and we present our response to each of them individually below. A marked-up manuscript version has also been embedded at the end of this document. We hope, our manuscript is acceptable for Annalese Geophysicae in this form.

Best regards

Sharon Aol

Below you find our point-by-point reply. For the convenience of the referees we have repeated in the response the relevant comments and then given our answers in blue text.

Response to Anonymous Referee #1 comments

Comment: Present work describes comparison of ionospheric irregularity data between the satellite SWARM electron densities and ground-based JULIA radar data and ionosonde data,using the data obtained over Peru from 2014 to 2018. In terms of identification of ionospheric irregularities, they found good similarities between the three different data set. Their final conclusion was that SWARM data can be used as a tool to indicate presence of plasma plumes and Spread F occurrence. The data sets used in the manuscript are interesting and comparison of them in terms of plasma bubble finding, or validation study for identification of the plasma irregularities, are useful. However, if one asks what is a new finding in this work I could not find anything. The authors could have a new aspect if they further discuss in the data analysis, I guess. Therefore my conclusion is that the present work will not be acceptable as a scientific paper without any further scientific new finding.

Response: We are glad that the referee finds the data sets used in our paper interesting and comparison of them in terms of plasma bubble finding, or validation study for identification of the plasma irregularities useful.

The main focus, findings and innovations may not have been demonstrated and highlighted clearly in our manuscript. In the revised version, we have improved on our article organization and put more description to highlight our findings. Below are the points we want to address in this study and these have been highlighted in the revised manuscript.Please see the detailed descriptions in the revised manuscript at the Line numbers indicated:

- The main focus of this study is to determine whether Swarm in situ observations can be used as indicators of the presence of plasma plumes and spread-F on the ground by comparing simultaneous observations of plasma plumes by the Jicamarca unattended long term investigations of the ionosphere and atmosphere (JULIA) radar, ionogram spread F generated from ionosonde observations installed at the Jicamarca Radio Observatory (JRO), and irregularities observed in situ by Swarm. The combined multi-instrument measurements provide a more integrated and comprehensive way to study the morphological structure, development, and seeding mechanism of ionospheric irregularities.
- It should be noted that although ionospheric irregularities have been studied extensively, uncertainties still exist in understanding their evolution because of their varying scale sizes (Abdu, 2001; Sripathi et al., 2008; Aa et al., 2020). In this regard, different instruments are limited to observing ionospheric irregularities of particular scale size (Sripathi et al., 2008; Aa et al., 2020). Therefore, coordinated observation of ionospheric irregularities using different instruments is an effective way to generate an integrated and comprehensive image for specifying ionospheric irregularities of different scale sizes (e.g, Sripathi et al., 2008; Cherniak et al., 2019; Aa et al., 2019, 2020).(see Pg.2 L.24-29)
- Most previous studies (e.g, Kelley et al., 2009; Siefring et al., 2009; Hysell et al., 2009; Roddy et al., 2010; Nishioka et al., 2011) have compared zonally oriented in situ plasma density measurements from Communication Navigation Outage Forecasting System (C/NOFS) satellite with JULIA observations. The Swarm satellites revisit neatly the same area in orbits oriented in the merdional direction. Therefore, our study compares sub-kilometer in situ ionospheric irregularities recorded by Swarm in the meridional direction with observations from Jicamarca. We found that the results based on the JULIA radar and ionosonde agreed with the plasma density obtained from measurements of the Swarm faceplate for single satellite passes over or near the JRO. (see Pg.3 L.1-7)

- Previous comparison of Swarm in situ measurements with ground-based radar observations (Zakharenkova et al., 2016, e.g,) mostly used LP measurements at 2 Hz frequency. The faceplate carried by Swarm as part of the Electric Field Instrument (EFI) has enabled the discovery of small-scale (down to 500 km length scale along the spacecraft track) ionospheric irregularities. In this study, we used Swarm faceplate measurements at a frequency of 16 Hz. Coherent scatter radars e.g, the JULIA radar can monitor irregularities at high spatial resolution (3 m scale length for the case of JULIA) and therefore these were compared with Swarm faceplate observations of ionospheric irregularities of small scales. The high-resolution faceplate data enabled smaller scale structures to be identified in electron density. Also, previous comparison of Swarm in situ measurements with ground-based radar observations (Zakharenkova et al., 2016, e.g,) were mostly single case presentations. Our study provides an extended statistical analysis covering years from 2014 to 2018.(see Pg.3 L.15-19)
- As far as we know, a quantitative statistical relationship between plasma bubbles observed in situ in the meridional direction, 250 MHz amplitude scintillation, and JULIA observations were reported by Burke et al. (2003) using data recorded by the polar-orbiting Defense Meteorological Satellite Program (DMSP). However, DMSP orbited at an altitude of about 840 km and this was a limitation in that most ionospheric irregularities didnot ascend to DMSP altitude. In our study, we used the polar orbiting Swarm satellites which has provided a renewed opportunity to compare in situ and JULIA observation at altitudes of 460 km (Swarm A and C) and 510 km (Swarm B). Compared to DMSP, Swarm allows comparison of measurements from identical instruments at different altitudes and in different longitudinal sectors. (see Pg. 3 L. 8-15)
- As far as we know, Wang et al. (2014) were among the first to make concurrent observations of strong range spread-F and ionospheric irregularities measured in situ using ROCSAT-1 satellite and they found that strong spread-F were caused by the ionospheric irregularities. However, ROCSAT-1 orbited at about 600 km altitude with 35° orbital inclination. Therefore, we also compared the JULIA and Swarm observations of ionospheric irregularities with spread-F signatures recorded by an ionosonde colocated with the JULIA radar.(see Pg. 3 L. 29-33)

Minor Comments:

Comment1: Page 4, line 29, “Ngwira et al. (2013a)”: change to“(Ngwira et al., 2013a)

Response: The citation has been changed as suggested. (see Page 5 line 11)

Comment2: Page 5, line 8, “Smith et al,„,”: change to “(Smith et al., 2015;Zhan et al. 2018)

Response: The citation has been changed as suggested. (see Page 5 line 20)

Comment3: Page 5, line 29, “from the left panel of Fig. 1”: change to “fromthe right panel of Fig. 1”

Response: The sentence has been changed as suggested by the referee. (see Page 6 line 6-7)

Comment4: Page 7, Figure 3: Please explain why the authors plotted themaximum ranges as a function of time (days). It seems to have no relation between themaximum range and Time(days).

Response: The maximum ranges were plotted to check the altitude coverage of the various types of plumes observed by the JULIA radar compared to the Swarm altitudes. The maximum ranges were obtained for each “day of the month” when the JULIA data was available. As identified by the referee, there indeed seems not be a direct relation between “Maximum range” and “Time (days)”. Instead each maximum range corresponds to “a day of the month”. Therefore, the x-label of Figure 3 has been changed to “Day of the month”. (see Fig. 3 Pg. 7)

Comment5: Page 12, Figure 7: The authors did not discuss in the case of “Irregularities observed by SWARM only”. According to the height coverage of Julia radar (90 to 800 km), any irregularities detected by SWARM should be detectedby Julia radar. It could be difference of threshold of detection amplitude (?), further discussion would be helpful for readers.

Response: Ideally, any irregularity detected by Swarm would be detected by JULIA depending on the proximity of the Swarm pass to the JULIA longitude and the magnitude of the irregularitiy. Given the longitudinal range (±5°) that was used for good statistical coverage (see Pg 10 Line 11), there were chances that Swarm would record ionospheric irregularities without JULIA identifying any plume structures. This is because ionospheric irregularities tend to be magnetic field aligned (Ossakow, 1979; Kil and Heelis, 1998; Nishioka et al., 2008; Kelley, 2009). An example is presented here in Figure 1. On the day 2015-11-08, Swarm encountered ionospheric irregularities,

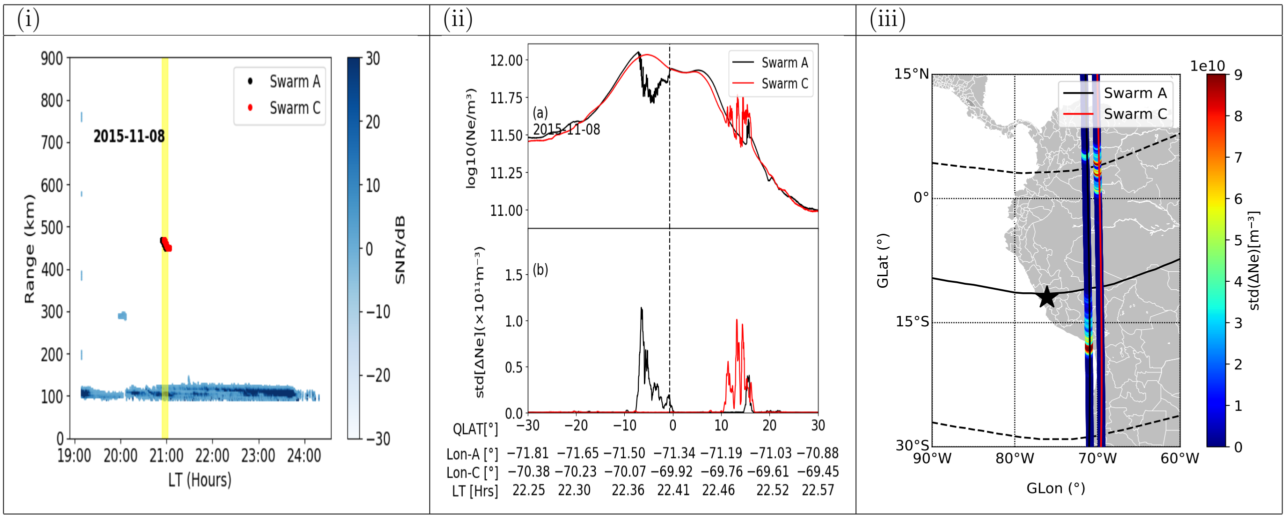

Figure 1. Example of collocated observation by Swarm and JULIA on 2015-11-08.

while JULIA recorded no plume structures. Clearly, the Swarm passes were offset from the JULIA longitude to the east. The following discussion has been added in the revised manuscript, to explain “Irregularities observed by SWARM only”

For instances when Swarm registered events, while JULIA and ionosonde recorded no signatures, we checked on the longitudinal separation between the satellite passes and the ground-site. The longitudinal separations obtained between the Swarm passes and the ground site were often $\approx 5°$ and the magnitude of the in situ perturbations were relatively low. Ionospheric irregularities tend to be magnetic field aligned (Ossakow, 1979; Kil and Heelis, 1998; Nishioka et al., 2008; Kelley, 2009) and therefore, Swarm may encounter irregularities in situ of relatively low magnitudes, while JULIA and ionosonde do not identify any events, for wider longitudinal offset of a pass from the ground site.(see Pg.11 L.19 -24)

Comment6: Page 16, line 1, “The Bragg condition”: Please explain what is “Bragg condition” for readers who are not familiar to the phrase.

Response: The Bragg condition explains the effect of periodic or quasi-periodic variations of the refractive index on the propagation of electromagnetic waves when the scales of the variations are of the order of the wavelength. The radio waves fulfilling the Bragg condition scatter at periodic variations of the refractive index such that a coherent superposition of reflections occurs and a reflected waves propagates in the direction of the radar receiver. The Bragg condition describes when the constructive interference occurs in a certain ratio between the transmitted wavelength and the distance of the reflective sub-surfaces:

$\mathrm{d} = \frac{\lambda_t}{2.\cos\theta}$

d=distance between maxima and minima of the refractive index

λ_t=transmitted wavelength

θ=incident angle

The following sentence has been included in the manuscript as further explanation of the “Bragg condition”:

> The Bragg condition for backscatter means that a radar can only observe structures in the refractive index with scale sizes close to the half radar wavelength (Kelley, 2009; Hocking et al., 2016).(see Pg. 17 L. 2-3)

Comment7: Page17, Conclusions, lines 13-14: “A few exceptions were also observed when,,,”: Furtherscientific discussion would be valuable for readers

Response: This has been addressed in response to **Comment5**.

In addition, the following sentences have been included in the conclusion as further discussion for the observation made in lines 13-14 of the previous version of the manuscript:

For the case when JULIA and ionosonde recorded irregularity signatures, while Swarm observed no structures, the plume structures may not have ascended to Swarm altitudes by the time the satellites passed over Jicamarca or the satellites were simply in a different location. Swarm was able to detect ionospheric irregularities in situ, while no signature was recorded on the ground because the irregularities occurred at magnetic longitudes which were largely offset from the longitude of the ground-site.(see Pg. 17 L. 27-32)

Response to Anonymous Referee #2 comments

General Comment: The authors compare density irregularities observed in-situ by the Swarm satellites with ground-based observations of plumes made by the Jicamarca unattended long term investigations of the ionosphere and atmosphere (JULIA) radar and ionosondes. Using data between 2014 and 2018, the authors investigate whether Swarm can be used as indicator of plasma plumes/Spread F observed on the ground. Showing a few case studies and by comparing the statistical trends between the in-situ and ground-based instruments, the authors conclude that Swarm can be used to detect the presence of well-developed plumes. The manuscript is carefully organized, the figures and presentation are clear, and the text is generally well written. While comparisons between in-situ and ground-based is worthwhile, and the datasets well suited, the novelty and importance of the findings are not significant enough, in my opinion. However, I think this work has potential values after significant additional work and resubmission. Suggestions and comments are given below.

Major Comments:

Comment 1: The author mention that their main focus is to determine whether Swarm can be used to detect plumes and Spread F. Even though previous studies used lower sampling resolution/single cases, I have difficulties understanding why the previous work(s) is(are) not sufficient to determine whether Swarm can detect plumes or not? There is even a standard Swarm data product called the Ionospheric Bubble Index (IBI) to detect equatorial irregularities (which does not seem to be referred to).

Response: The differences between this work and the previous works may not have been demonstrated and highlighted clearly in our manuscript. In the revised version, we have put more description to highlight this. Below are the points we want to address in this study:

- Most previous studies (e.g, Kelley et al., 2009; Siefring et al., 2009; Hysell et al., 2009; Roddy et al., 2010; Nishioka et al., 2011) have compared zonally oriented in situ plasma density measurements from Communication Navigation Outage Forecasting System (C/NOFS) satellite with JULIA observations. The Swarm satellites revisit neatly the same area in orbits oriented in the merdional direction. Therefore, our study compares sub-kilometer in situ ionospheric irregularities recorded by Swarm in the meridional direction with observations from Jicamarca.(see Pg.3 L. 2-7)
- Previous comparison of Swarm in situ measurements with ground-based radar observations mostly used LP measurements at 2 Hz frequency (e.g, Zakharenkova et al., 2016). In this study, we used Swarm faceplate measurements at a frequency of 16 Hz. The faceplate carried by Swarm as part of the Electric Field Instrument (EFI) has enabled the discovery of small-scale (down to 500 km length scale along the spacecraft track) ionospheric irregularities. Coherent scatter radars e.g, the JULIA radar can monitor irregularities at high spatial resolution (3 m scale length for the case of JULIA) and therefore these were compared with Swarm faceplate observations of ionospheric irregularities of small scales. The high-resolution faceplate data enabled smaller scale structures to be identified in electron density. Also, previous comparison of Swarm in situ measurements with ground-based radar observations (e.g, Zakharenkova et al., 2016) were mostly single case presentations. Our study provides an extended statistical analysis covering years from 2014 to 2018.(see Pg. 3 L. 15-19)
- As far as we know, a quantitative statistical relationship between plasma bubbles observed in situ in the meridional direction, 250 MHz amplitude scintillation, and JULIA observations were reported by Burke et al. (2003) using data recorded by the polar-orbiting Defense Meteorological Satellite Program (DMSP). However, DMSP orbited at an altitude of about 840 km and this was a limitation in that most ionospheric irregularities didnot ascend to DMSP altitude. In our study, we used the polar orbiting Swarm satellites which has provided a renewed opportunity to compare in situ and JULIA observation at altitudes of 460 km (Swarm A and C) and 510 km (Swarm B). Compared to DMSP, Swarm allows comparison of measurements from identical instruments at different altitudes and in different longitudinal sectors. (see Pg. 3 L. 8-15)

– Concerning the IBI index, it is a standard Level 2 product of the Swarm mission (Park et al., 2013). IBI provides information on climatology of ionospheric irregularities itself as well as on the disturbance level of the magnetic

field data by taking both electron density and magnetic field measurements into account. Following the referees suggestion, we accessed the IBI index for all the Swarm satellites from
https://swarm-diss.eo.esa.int/#swarm%2FLevel2daily%2FLatest_baselines%2FIBI and generated the distribution of ionospheric irregularities derived from the IBI as a function of quasi-dipole latitude and Local time. The results for Swarm C are presented here in Fig. 2. It is important to note that the IBI is just

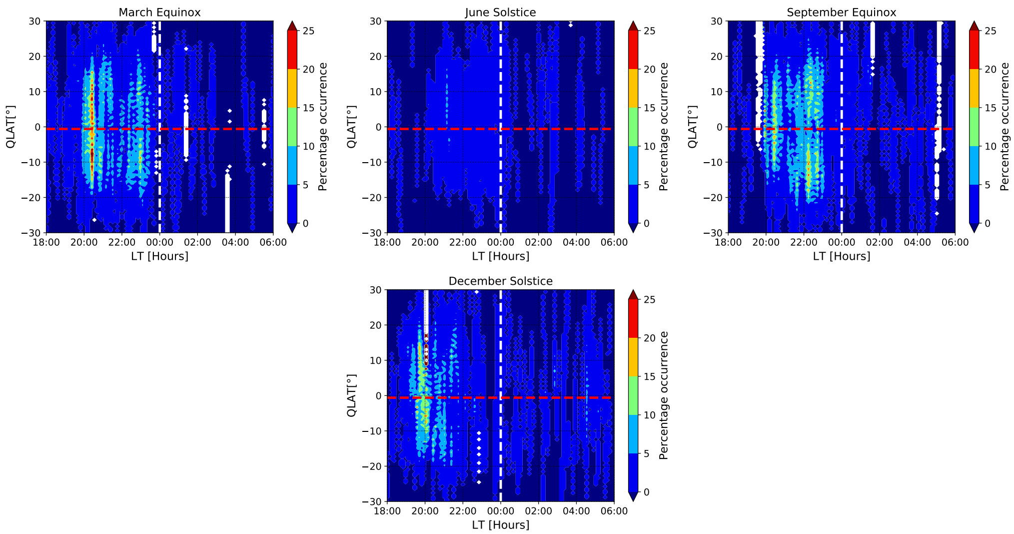

Figure 2. Distribution of ionospheric irregularities derived from the IBI as a function of quasi-dipole latitude and Local time for Swarm C.

either 1, 0, -1 for bubble detected, not detected or undetermined, respectively. Therefore, to generate the results in the figure, the datasets were first grouped into different seasons corresponding to March Equinox (Feb-Mar-Apr), June Solstice (May-Jun-Jul), September Equinox (Aug-Sep-Oct), and December Solstice (Nov-Dec-Jan). For each season, the data was then binned into $1^\circ \times 0.1$ hr quasi-dipole latitude-local time bin. For each quasi-dipole latitude-local time bin, the percentage occurrence was obtained by dividing the number of observations with $\mathrm{IBI} = 1$ by the total number of observations. The distribution of ionospheric irregularities derived from the IBI shows similar seasonal dependence to the ones shown in Figure 11(see manuscript), with highest percentage occurrence in the equinoxes and December solstice. The latitude-LT plots of IBI do not offer as much details as the density measurements. However, the comparison reveals also differences. While the absolute irregularity strength largely shows the familiar double peaks at roughly $\pm 15^\circ$ north and south of the magnetic equator, the IBI has almost no clear double structure and reflects only periods with very strong irregularities. The reliability of IBI as an indicator of Spread F and scintillations of radio signals seems doubtful to us.

– It is interesting to know how ionospheric irregularities are classified by the plasma bubbles detection algorithm. Therefore, we have added the IBI index analysis in the revised version of the manuscript. (see Pg 16. L.3-15 and Figure. 12)

Comment 2: I agree that statistical studies can provide additional information. However, it is not clear to me what the authors actually get from their statistics, except for similar trends as the ones published in the literature (both from ground-based and Swarm "irregularity" studies). I am fairly certain that with their interesting dataset, the authors can reach more substantial conclusions, especially with the spatial/altitudinal separation and sampling rate of Swarm.

Response: Concerning the observations and conclusions from the statistical analysis, these may not have been demonstrated and highlighted clearly in our manuscript.

- Specifically for Fig. 7, the effect of spatial and altitudinal separation among the Swarm satellites can be observed and the following observations and conclusions have been added in the revised manuscript in this regard:
  - For instances when Swarm registered events, while JULIA and ionosonde recorded no signatures, we checked on the longitudinal separation between the satellite passes and the ground-site. The longitudinal separations obtained between the Swarm passes and the ground site were often $\approx 5°$ and the magnitude of the in situ perturbations were relatively low. Ionospheric irregularities tend to be magnetic field aligned (Ossakow, 1979; Kil and Heelis, 1998; Nishioka et al., 2008; Kelley, 2009) and therefore, Swarm may encounter irregularities in situ of relatively low magnitudes, while JULIA and ionosonde do not identify any events, for wider longitudinal offset of a pass from the ground site.(see Pg. 11 L. 19-25)
  - In addition, for irregularities observed by Swarm only, Swarm B had the lowest percentage occurrence close to about 5% compared to Swarm A/C. The observed difference may be because of the progressive temporal and altitudinal separation between Swarm B and A/C (Zakharenkova et al., 2016). Swarm B orbits at a higher altitude compared to A/C and it crosses the same region later than A/C. Generally, in Fig. 7, a difference in percentage occurrence in all categories is observed between Swarm A and C although they orbit at the same altitude above sea-level. The large scale longitudinal bubble structure is sometimes observed with the two Swarm satellites (Xiong et al., 2016), but for small scale irregularities, the 1.5° longitudinal separation between the satellites is too large for a significant correlation between them.(see Pg. 12 L. 1-7)

Comment 3: (section 3.3) The description of the method to calculate the statistics (selection of events, number of events, how occurrence rates are calculated, exact months, description of quantities shown in figures etc.) is insufficient.

Response: The description of the method to calculate the statistics may not have been described in detail. In the revised manuscript, we have incorporated detailed description of the methods we adopted. Below is the methods we used in the statistical analysis:

- For Section 3.3.1
  - The Swarm satellites regress in longitude by about 22.5° between orbital ascending nodes. Therefore, in comparison with JULIA and ionosonde data, the Swarm passes were allowed to be within ±5° magnetic longitude of the JRO to make sure that a sufficient amount of Swarm passes could be used for the statistical examination. Summary plots such as those presented in Fig. 4 were generated for all days during the years from 2014 to 2018 for which the data was available. In total, 560 night-time orbits were used for which JULIA, Swarm, and ionosonde data were available concurrently. The outputs of the summary plots could be categorized into four cases considering the presence (or not) of irregularities. In general, these four cases are: Irregularities observed both on the ground and in situ, No irregularities observed both on the ground and in situ, Irregularities observed only in situ, and Irregularities observed only on the ground. For each RTI plot, the SNR corresponding to the peak height was determined and an event was identified as a significant irregularity when the peak height was ≥ 400 km. For peak height less than 400 km, these were classified as no irregularities. For the in situ Swarm observations, we considered a threshold of $1 \times 10^{10}\ \mathrm{m}^{-3}$ for std(ΔN_e) as a significant irregularity event, while for std(ΔN_e) less than the threshold were considered as no irregularities. For the ionosonde measurements, QF values greater than or equal to 20 km were considered as significant irregularity events. For each category, the percentage occurrence was computed as a ratio of the total number events in that category to the number of observations.(see Pg. 10 L. 10-17 and Pg. 11 L. 1-6)
- For Section 3.3.2:
  - To obtain the results presented in Fig. 10, ground-based JULIA SNR data for the years from 2014 to 2018 were used. To eliminate the impact of geomagnetically disturbed conditions on the statistical outcomes, the data were filtered and only those recorded during quiet geomagnetic conditions ($\mathrm{Kp} \leq 3$) were taken into account. The JULIA data accumulated for the years from 2014 to 2018 were sufficient for examining the seasonal variation. Therefore, the seasonal dependence of local time distribution of JULIA observations of ionospheric irregularities was also examined by grouping all the data into different seasons corresponding

to March Equinox (Feb-Mar-Apr), June Solstice (May-Jun-Jul), September Equinox (Aug-Sep-Oct), and December Solstice (Nov-Dec-Jan). For each local time-height bin, the percentage occurrence was obtained by dividing the number of observations with $\mathrm{SNR} > 10$ dB by the total number of observations (Smith et al., 2016). (see Pg. 12 L. 14-16 and Pg. 13 L. 1-6)

- Figure 10 shows the QF indices derived from ionosonde observations as a function of local time and months. To obtain the results presented in Fig. 10, ground-based ionosonde data for the years from 2014 to 2018 were also used. The data were also filtered and only those recorded during quiet geomagnetic conditions were considered. To generate the results presented in Figure 10, for each month (y-axis), the QF indices were averaged over 1 hr Local time bins. (see Pg. 14 L. 12-17)
- Figure 11 shows the QLat-LT distributions of std(ΔN_e) for the Swarm satellites for the years from 2014 to 2018. Recall that the Swarm passes were allowed to be within $\pm 5°$ magnetic longitude and $\pm 40°$ QLat. The results presented in Fig. 11 were also generated considering only the geomagnetically quiet conditions ($\mathrm{Kp} \leq 3$). The N_e data collected for the five years were also grouped into different seasons similar to those presented in Fig. 9. The std(ΔN_e) was then calculated in bins of $1° \times 0.1$ hr resolution in QLat and Local time. The occurrence rate of ionospheric irregularities does not always correspond to the highest amplitude of irregularity structures (Wan et al., 2018). Therefore, we presented the calculated std(ΔN_e) per bin as a function of QLat and Local time as seen in Fig. 11.

Minor Comments:

P.3 l.30: Doesn't the faceplate actually record Ni, from which Ne is calculated?

Response: Ion density, N_i is derived from the faceplate current assuming that the current is carried by ions hitting the faceplate due to the orbital motion of the spacecraft. However, due to quasi-neutrality N_i must be equal to the electron density N_e (Buchert, 2016).

This has been added in the revised manuscript for clarification. (see Pg. 4 L. 10-13)

P.4 l.18: "vs" should be "versus"

Response: This has been changed as suggested. (see Pg. 4 L. 33)

P.4 l.29: "Ngwira et al. (2013)" should have (. . .)

Response: The citation identified has been changed as suggested. (see Pg. 5 L. 11)

P.4 l.30: Is the standard deviation also calculated on a 2sec running window? Are the scales selected important for you results?

Response: The standard deviation of the residuals was calculated at a running window of 2-s and this was used to represent the magnitude of the electron density perturbation.

This information has been added in the revised manuscript.(see Pg. 5 L. 12)

Concerning the scales selected, it is important for our results since we concentrated on small-scale ionospheric irregularities. The window to calculate dN_e and the standard deviation (for the case of small-scale ionospheric irregularities) should be short, but long enough to avoid spurious detection of ionospheric irregularities. We also tried 1 s, 16 points, instead of 2s, 32 points, and the outcome was similar and reasonable.

In addition, the Coherent scatter radars e.g, the JULIA radar can monitor irregularities at high spatial resolution (3 m scale length for the case of JULIA) and therefore these were compared with Swarm faceplate observations of ionospheric irregularities of small scales which were quantified by using a running window of 2-s.

P.5 l.7: "Smith et. Al (2015); Zhan et al. (2018)" should have (. . .)

Response: The citations identified have been changed as suggested. (see Pg. 5 L 20)

P.5 l.12: Definition of ISR.

Response: ISR stands for Incoherent Scatter Radar. This has been added in the revised manuscript. (see Pg. 5 L 24)

P.5 l.14: How exactly do the authors define "nighttime”?

Response: In our manuscript, nighttime is defined as the time period between 1800 LT and 0600 LT. The sentence has been rephrased in the revised manuscript to make this clear as follows:

Therefore, to compare the Swarm observations with the JULIA measurements, only swarm satellite passes for the time period between 1800 LT and 0600 LT were considered. (see Pg. 5 L 27)

P.5 l.19: Space between "explorer" and (Galkin. . .)

Response: This has been adjusted as suggested. (see Pg. 5 L 32)

P.5 l.28: Definition of “QLat”.

Response: QLat stands for quasi-dipole latitude (Laundal and Richmond, 2016). This has been added in the revised manuscript. (see Pg. 6 L 5)

P.5 l28: “Much higher altitude”. This is very subjective.

Response: The identified words have been removed from the revised manuscript and the sentence has been rephrased to:

Also, Swarm B which orbited at about 510 km altitude above sea level recorded ionospheric irregularity structures on 2015-04-05 as seen from the right panel of Fig. 1.(see Pg. 6 L 6-7)

P.7 Figure 3. This figure and the explanation are not clear: do the authors bin the data by day of the month, and take the maximum for each day over 4 years?.

Response: The maximum ranges were obtained for each “day of the month” over the four years when the JULIA data was available. As identified by the referee, there indeed seems not to be a direct relation between “Maximum range” and “Time (days)”. Instead each maximum range corresponds to “a day of the month”. Therefore, the x-label of Figure 3 has been changed to “Day of the month”. (see Fig. 3 in the revised manuscript)

P.8 l.14: Definition of “EIA”.

Response: EIA stands for Equatorial Ionization Anomally. This has been added in the revised manuscript. (see Pg.8 L 11)

P.8 l 30: “20.05 LT to 21:00 LT” I don’t read the same time interval from the Figure.

Response: To make it clearer, the x-axis tick labels for LT have been changed to LT(hh:mm) in the revised manuscript as shown here in Fig. 3: To be exact, the time interval have been changed to 20:27 LT to 21:05 LT, in the revised manuscript. (see Pg. 9 L. 16)

P.15-16 Figure 10 and Figure 11: Could the authors describe in more detail how those figures are obtained?

Response: This has been discussed in response to major comment 3.

P.16 l.2: Didn’t the authors use the 16 Hz? (Why is 2 Hz relevant here?)

Response: Since we concentrated on the 16 Hz N_e, in the revised manuscript, the sentence has been rephrased to:

- The Swarm electron density measurements used in this study are limited by the sampling rate of 16 Hz and the orbital velocity of about 7.5 km/s to wavelengths of about 500 m, respectively, and longer. (see Pg. 17 L. 3-5)

P.17. l.1-3: The purpose of these sentences is unclear to me. It is well known that equatorial irregularities can cause scintillations.

Response: The sentence has been removed in the revised manuscript.

P.17 l.12: “directory” – “directly”?

Response: This has been changed in the revised manuscript as suggested by the reviewer.(see Pg. 17 L. 24)

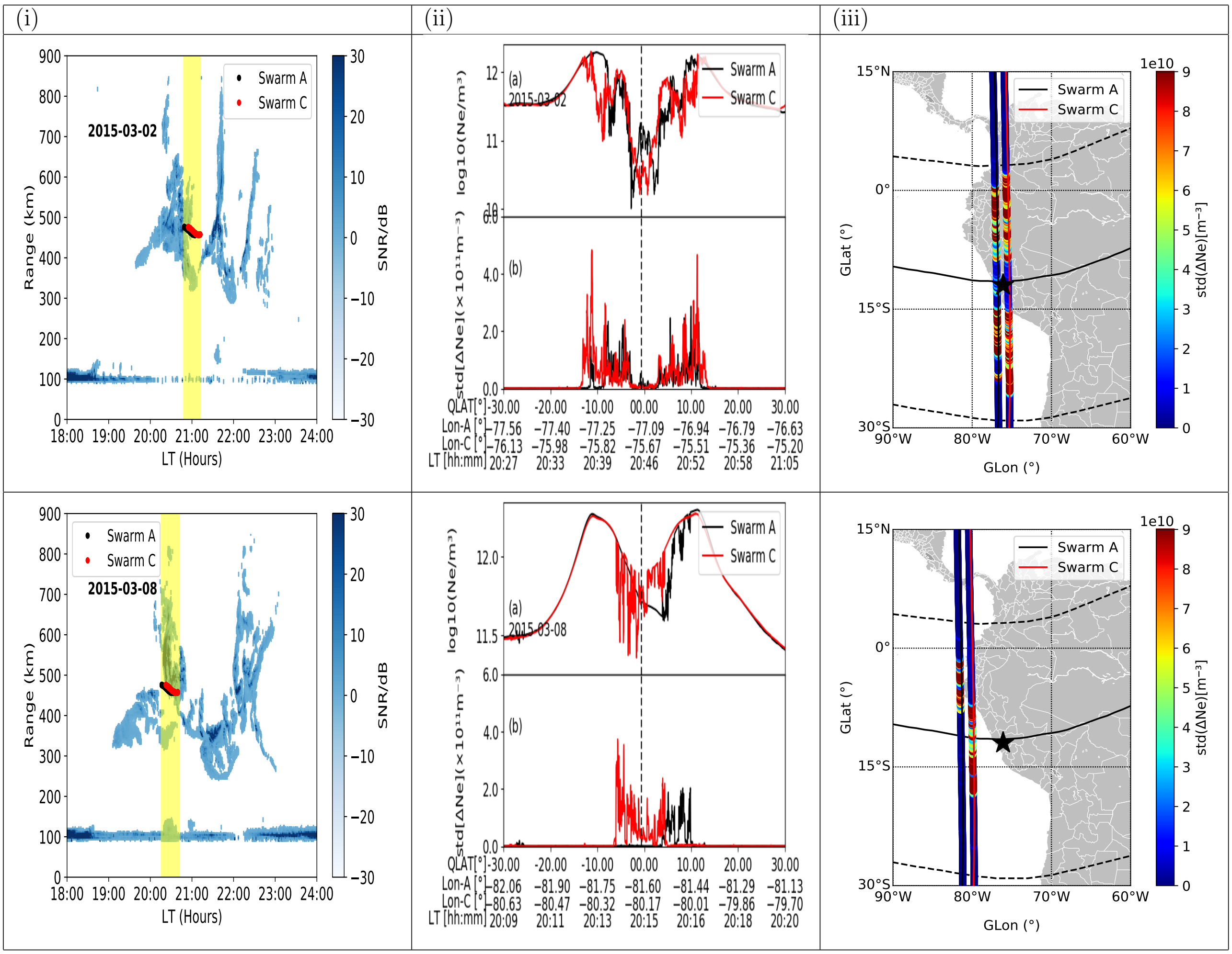

Figure 3. Examples of collocated observations by Swarm and JULIA radar on 2015-03-02 and 2015-03-08.

Simultaneous Ground-based and In Situ Swarm Observations of Equatorial F-region Irregularities over Jicamarca

Sharon Aol[1], Stephan Buchert[2], Edward Jurua[1], and Marco Milla[3]

[1]Mbarara University of Science and Technology, Mbarara, Uganda

[2]Swedish Institute of Space Physics, Uppsala, Sweden

[3]Radio Observatorio de Jicamarca, Instituto Geofísico del Perú, Lima, Peru

Correspondence: Sharon Aol (saol@must.ac.ug)

Abstract. Ionospheric irregularities are a common phenomenon in the low latitude ionosphere. They can be seen in situ as depletions of plasma density, radar plasma plumes or ionogram spread F by ionosondes. In this paper, we compared simultaneous observations of plasma plumes by the Jicamarca unattended long term investigations of the ionosphere and atmosphere (JULIA) radar, ionogram spread F generated from ionosonde observations installed at the Jicamarca Radio Observatory (JRO), and irregularities observed in situ by Swarm, to determine whether Swarm in situ observations can be used as indicators of the presence of plasma plumes and spread-F on the ground. The study covered the years from 2014 to 2018 when all the data-sets were available. Overall, the results showed that Swarm's in situ density fluctuations on magnetic flux tubes passing over (or near) the JRO may be used as indicators of plasma plumes and spread-F over (or near) the observatory. For Swarm and the ground-based observations, a classification procedure was conducted based on the presence or absence of ionospheric irregularity structures. There was a strong consensus between ground-based observations of irregularity structures and Swarm's depth of disturbance of electron density for most passes. Cases, where irregularity structures were observed on the ground with no apparent variation in the in situ electron density or vice versa, suggest that irregularities may either be localized horizontally or restricted to particular height intervals. The results also showed that the Swarm and ground-based observations of ionospheric irregularities had similar local time statistical trends with the highest occurrence obtained between 20:00 and 22:00 LT. Also, similar seasonal patterns of occurrence of in situ and ground-based ionospheric irregularities were observed with the highest percentage occurrence in December Solstice and Equinoxes and low occurrence in June Solstice. The observed seasonal pattern was explained in terms of the pre-reversal enhancement (PRE) of the vertical plasma drift. Initial findings from this research indicate that fluctuations of in situ density observed meridionally along magnetic field lines passing through JRO can be used as an indication of the existence of well-developed plasma plumes.

Keywords. Equatorial Ionosphere, Ionospheric Irregularities

1 Introduction

Generally, the ionosphere can be viewed as a layer with a relatively uniform plasma density distribution (Ngwira et al., 2013b). However, the nighttime low latitude ionosphere is characterized by localized plasma density structures, known as ionospheric irregularities (Stolle et al., 2006). The equatorial ionospheric irregularities may be identified as irregular plasma density bite outs observed in situ along Low Earth Orbit (LEO) satellite tracks in the topside ionosphere (Woodman and La Hoz, 1976; Tsunoda, 1980; Tsunoda et al., 1982; Kelley, 2009). Ionospheric irregularities may also manifest as Equatorial Spread Fs (ESF) which are irregular signatures on ionograms due to backscattering from and above the F-layer at the bottom (Woodman and La Hoz, 1976; Hysell and Burcham, 1998). Ionospheric irregularities have also been called plasma plumes because of their appearance in range versus time radar displays (Woodman and La Hoz, 1976). The plumes are characterized by elongated, wedge-like cross-sections that extend from the bottom of the F-layer to higher altitudes (Tsunoda, 1980; Tsunoda et al., 1982; Ma and Maruyama, 2006). Ionospheric irregularities usually extend along magnetic field lines to magnetic latitudes of about $\pm 15° - \pm 20°$ (Ossakow, 1979; Kil and Heelis, 1998; Nishioka et al., 2008; Kelley, 2009).

Ionospheric irregularities in the low latitudes arise after sunset because of the Rayleigh - Taylor Instability (RTI) which originates from the lower F - region (Woodman and La Hoz, 1976; Kelley, 2009; Schunk and Nagy, 2009). These irregularities vary in scale size, between several centimeters and hundreds of kilometers (Tsunoda et al., 1982). A width of about 100 km was observed for the depleted ESF bands using an all-sky air-glow imager (Otsuka et al., 2004). The occurrence of ionospheric irregularities varies according to local time, season, longitude, latitude, solar and magnetic activity (Kil et al., 2009). Their occurrence is a subject of interest because of the effect they have on propagating radio signals. Their presence in the ionosphere may cause amplitude and phase scintillations of radio signals, thereby affecting many applications that rely on these signals (Yeh and Liu, 1982).

Equatorial ionospheric irregularities have been observed many times using ground-based instruments such as incoherent and coherent scatter radars, ionosonde, airglow cameras and space-based instruments such as rockets and LEO satellites (e.g, Woodman and La Hoz, 1976; Hysell et al., 1997; Nishioka et al., 2008; Fejer et al., 1999; Burke et al., 2003; Sripathi et al., 2008; Wang et al., 2015; Hickey et al., 2018; Aa et al., 2020). It should be noted that although ionospheric irregularities have been studied extensively, uncertainties still exist in understanding their evolution because of their varying scale sizes (Abdu, 2001; Sripathi et al., 2008; Aa et al., 2020). In this regard, different instruments are limited to observing ionospheric irregularities of particular scale size (Sripathi et al., 2008; Aa et al., 2020). Therefore, coordinated observation of ionospheric irregularities using different instruments is an effective way to generate an integrated and comprehensive image for specifying ionospheric irregularities of different scale sizes (e.g, Sripathi et al., 2008; Cherniak et al., 2019; Aa et al., 2019, 2020). Particularly, the Jicamarca Radio Observatory (JRO) has provided a rare opportunity to observe ionospheric irregularities using multiple ground-based instruments because of its strategic location (12.0°S, 76.8°W; magnetic latitude 0.6°S) at the magnetic equator. Many studies have reported the connection between scintillation producing irregularity structures observed by JULIA and Equatorial Plasma Bubbles (EPBs) observed in situ over Jicamarca (e.g, Morse et al., 1977; Basu et al., 1980; Hysell and Burcham, 2002; Burke et al., 2003; Kelley et al., 2009; Siefring et al., 2009; Roddy et al., 2010; Nishioka et al., 2011, etc). However, the relationship between meter-scale irregularities detected by coherent scatter radars to the underlying state parameters of the ionospheric plasma is not yet well understood (Hysell et al., 2009). Previous studies (e.g, Kelley et al., 2009; Siefring et al., 2009; Hysell et al., 2009; Roddy et al., 2010; Nishioka et al., 2011, etc) have mostly compared zonally oriented in situ plasma density measurements from Communication Navigation Outage Forecasting System (C/NOFS) satellite with JULIA observations. The European Space Agency's (ESA's) Swarm satellites revisit neatly the JRO in orbits oriented in the meridional direction, providing a renewed opportunity to study in situ ionospheric irregularities recorded by Swarm in the meridional direction in comparison with observations from Jicamarca.

A quantitative statistical relationship between plasma bubbles observed in situ in the meridional direction, 250 MHz amplitude scintillation, and JULIA observations were reported by Burke et al. (2003) using data recorded by the polar-orbiting Defense Meteorological Satellite Program (DMSP). From the observations made by Burke et al. (2004), the plasma plumes recorded by JULIA frequently occurred at altitudes lower than that of the DMSP orbit. Most of the plasma plumes failed to reach altitudes >600 km and therefore, they were not observed by DMSP satellite which orbited at an altitude of about 840 km. It is possible compare in situ measurements made by Swarm and JULIA observation at altitudes of 460 km (Swarm A and C) and 510 km (Swarm B). Compared to DMSP, Swarm allows comparison of measurements from identical instruments at different altitudes and in different longitudinal sectors (Zakharenkova et al., 2016). Previous comparison of Swarm in situ measurements with ground-based radar observations (e.g, Zakharenkova et al., 2016) mostly used LP measurements at 2 Hz frequency. The faceplate carried by Swarm as part of the Electric Field Instrument (EFI) has enabled the discovery of small-scale (down to 500 km length scale along the space-craft track) ionospheric irregularities. Also, previous comparison of Swarm in situ measurements with ground-based radar observations was mostly a single case presentations. Zakharenkova et al. (2016) demonstrated that the gradual spatial separation between Swarm A, C and B would decrease the likelihood that all three satellites could capture ionospheric irregularity signatures in the same localized region or near a particular equipment installed on the ground such as ionosonde, radars, etc. Nevertheless, only one single case of comparison between Swarm and JULIA observation was provided by Zakharenkova et al. (2016).

In this paper, we quantitatively compared the in situ observations of ionospheric irregularities recorded by the Swarm satellites with ground-based measurements of plasma plumes made by the JULIA radar for the years from 2014 to 2018, to determine whether Swarm in situ observations can be used as indicators of the presence of plasma plumes and spread-F on the ground. The comparison is complemented with ionosonde measurements of spread-F over JRO. Booker and Wells (1938) noted echo signatures on ionograms generated from ionosonde measurements and they suggested that these echo signatures arise from F region ionospheric irregularities. As far as we know, Wang et al. (2015) were among the first to make concurrent observations of strong range spread-F and ionospheric irregularities measured in situ using ROCSAT-1 satellite and they found that strong spread-F were caused by the ionospheric irregularities. However, ROCSAT-1 orbited at about 600 km altitude with 35° orbital inclination. Therefore, we also compared the JULIA and Swarm observations of ionospheric irregularities with spread-F signatures recorded by an ionosonde colocated with the JULIA radar. To understand the range of altitude above sea level where ionospheric irregularities occur and the effect they have on ground observations, a comparison of in situ electron density variation with ground-based measurements over a long time is essential.

This paper is organized in the following order: In Sect. 2, the data and methods used in this study are described. In Sect. 3, the results are presented and discussed. The findings of this study are summarized in Sect. 4.

2 Data and Methods

2.1 Data

This section provides brief descriptions of the instruments and data-sets used in this study to examine the signatures of ionospheric irregularities. In this study, we analyzed data obtained from Swarm, JULIA radar and ionosonde.

2.1.1 Swarm Measurements of Electron Density

The Swarm mission consists of three polar-orbiting satellites i.e., Swarm A, B, and C (Friis-Christensen et al., 2006). They were launched in near-polar orbits at an initial altitude of about 500 km on 22 November 2013 (Xiong et al., 2016; Wan et al., 2018). Each satellite is equipped with an Electric Field Instrument (EFI) which is mounted on the ram side of the spacecraft (Friis-Christensen et al., 2006; Knudsen et al., 2017). The ion density is derived from the EFI faceplate current assuming that the current is carried by ions hitting the faceplate due to the orbital motion of the spacecraft (Buchert, 2016). However, due to quasi-neutrality N_i must be equal to the electron density N_e. With the 16 Hz N_e measurements, Swarm observes irregularity structures with scale sizes of up to 500 m. Friis-Christensen et al. (2006) and Knudsen et al. (2017) provide detailed information on Swarm and onboard instruments. In this study we used, the 16 Hz N_e measurements to examine topside irregularity structures. The faceplate N_e data is readily available at `http://earth.esa.int/swarm`.

2.1.2 The JULIA Radar

The JULIA radar is a PC-based system for data acquisition. JULIA uses low-power transmitters with a frequency of approximately 50 MHz and Jicamarca's main antenna (Hysell and Burcham, 1998, 2002; Burke et al., 2003). It was designed to observe equatorial plasma irregularities and neutral atmospheric waves for extended periods of time. It is programmed to emit pulses of 26.6 μs duration at a repetition rate of 100 Hz (Burke et al., 2003). This allows sampling of 200 range gates of 4 km extent from 95 to about 900 km altitude above sea level (Hysell and Burcham, 1998). The pulse width used in the JULIA experiments in 2016 and 2018 was 25 μs and the pulse repetition was 160 pulses per second. In addition, 248 range gates of 3.75 km separation were sampled, going from 0 km to about 930 km. For the identification of 3 m-scale ionospheric irregularities, the back-scattered 50 MHz JULIA radar echo was used. The radar observations provide the Signal to Noise Ratio (SNR), Doppler velocity and spectral width as a function of height and time. Data collected by the JULIA radar is readily available at `http://jro.igp.gob.pe/madrigal/`. The website has JULIA data from 1996 till to-date. Our analysis was restricted to the years from 2014 to 2018 when JULIA, Swarm, and ionosonde data-sets were available.

2.1.3 The Digital Ionosonde

The Equatorial Spread F (ESF) signatures are often recorded by ionosondes installed in the JRO. The ionosonde at the JRO is a Digisonde DPS-4 (Reinisch et al., 1998) which records ionograms (altitude versus frequency plots) at 15 min intervals. The ionograms are systematically scaled by the Automatic Real-Time Ionogram Scaler with True height (ARTIST) UML ionogram autoscaling method, which extracts plasma frequency profiles versus altitude (Reinisch et al., 2005; Zhang et al., 2015). From the ionograms, the equatorial spread-F signatures were examined. The ionosonde data are also available on the Madrigal website and we used all the Jicamarca ionograms for the years from 2014-2018.

2.2 Methods

This section presents the analysis techniques used in this study to identify the observed ionospheric irregularity signatures using Swarm, JULIA and ionosonde.

2.2.1 In situ Ionospheric Irregularity Identification

To examine topside ionospheric irregularities, the 16 Hz N_e Swarm faceplate data were used. We followed the same method as Huang et al. (2014) and Ngwira et al. (2013a) to derive the absolute electron density perturbation along Swarm orbital tracks, but we focused mainly on small-scale equatorial plasma structures. We utilized a 2-s running mean filter to determine the mean N_e. The selected running mean is equivalent to a 15 km scale length, given Swarm's velocity of about 7.5 km/s. The mean N_e was subtracted from the original observations to get the residual, ΔN_e (Ngwira et al., 2013a). The standard deviation of the residuals was then calculated at a running window of 2-s to represent the magnitude of the perturbation (std(ΔN_e)). There is no standard threshold definition of how large std(ΔN_e) must be to identify plasma irregularities (Huang et al., 2014; Wan et al., 2018). However, the period considered in this study was characterized by low solar activity and the recorded ionospheric irregularities were very weak. Therefore, a threshold value of std(ΔN_e)=1×10^{10} m^{-3}, similar to that adopted by Huang et al. (2014), has been selected to provide a reasonable irregularity event identification at small scales and the relatively low Swarm altitudes during the study period.

2.2.2 Ground-based Ionospheric Irregularity Identification

The JULIA system computes and stores measurements of the zeroth and first lags of the auto-correlation function (ACF) of the signals from two receivers connected to the east and west quarters of the main antenna (Smith et al., 2015; Zhan et al., 2018). From these measurements, the total power, first moment Doppler velocity, and Doppler spectral width of the scattered signals can be estimated (Hysell et al., 1997; Hysell and Burcham, 1998). Of particular interest was the SNR measurements derived by the JULIA system to check plasma plumes for a given evening. Besides, we also used the vertical plasma drift measurements made by the Jicamarca Incoherent Scatter Radar (ISR) to examine the pre-reversal enhancement (PRE) drifts (Fejer et al., 1996; Smith et al., 2016). Field-aligned irregularities in the F-region are often observed between 1800 LT and 0600 LT by the JULIA radar. Therefore, to compare the Swarm observations with the JULIA measurements, only swarm satellite passes for the time between 1800 LT and 0600 LT were considered.

The comparison of JULIA and Swarm observations were supplemented with ionosonde measurements from the JRO. The ionosonde data analysis was carried out using the SAO Explorer software (Reinisch et al., 2005). To display ionograms, both the raw and processed (SAO) data were loaded into the SAO Explorer software. In addition, the spread-F index QF, known as the mean spread of the diffusing F layer trace, was obtained by the ARTIST directly from the ionograms using the SAO explorer (Galkin et al., 2008; Zhang et al., 2015) and this was also used in this study to analyze the spread-F signatures. The mean range spread refers to the averaged spread range of all frequencies that detect a diffuse echo in an ionogram (Zhang et al., 2015). The spread range at each frequency is the virtual height difference between the top and bottom of the spread echo at a particular frequency (Abdu et al., 2012; Zhang et al., 2015). The QF is assigned to NaN (not a number) if there is no spread F observed in an ionogram (Zhang et al., 2015). In the following section, the results of this study are presented and discussed.

3 Results and Discussions

3.1 Observations of Ionospheric Irregularities

Examples of ionospheric irregularity events observed by Swarm A, C on 2015-03-09 and B on 2015-04-05 are shown in Fig. 1. From the left panel of Fig. 1, Swarm A, C encountered ionospheric irregularity structures along their tracks occurring between

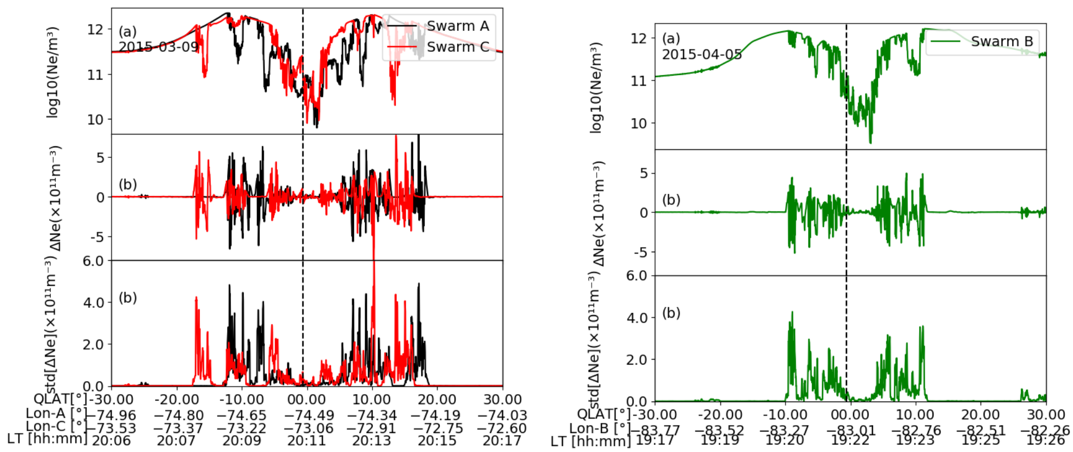

Figure 1. Swarm Faceplate N_e data of ionospheric irregularity events on 2015-03-09 and 2015-04-05. The panels show: (a) the N_e variation, (b) ΔN_e, and (c) std(ΔN_e) as functions of QLat, longitude (LON), and local time (LT). The dashed vertical black line represents the approximate QLat of JRO.

about $\pm 10^\circ - \pm 20^\circ$ quasi-dipole latitude (QLat) (Laundal and Richmond, 2016), while they orbited over JRO on 2015-03-09. Also, Swarm B which orbited at about 510 km altitude above sea level recorded ionospheric irregularity structures on 2015-04-05 as seen from the right panel of Fig. 1. Panel (b) of Fig. 1 presents the ΔN_e with background variations subtracted. Figure 1(c) shows how well the quantified absolute density perturbation captured the small-scale ionospheric irregularities in the faceplate N_e measurements. Given the fact that the irregularities structures were observed in situ at Swarm altitudes, this shows that these irregularity structures were in the topside ionosphere. The observed ionospheric structures occurred post-sunset and they are certainly because of the generalized RTI (Kelley, 2009).

The coherent scatter radar observations of ionospheric plasma irregularities are often shown in Range-Time-Intensity format in which the SNR is plotted against altitude (range) and time (Woodman and La Hoz, 1976; Hysell and Burcham, 1998). The major categories of plasma plumes that have been observed by the JULIA radar are Bottom-type, Bottom-side, and Topside (e.g, Woodman and La Hoz, 1976; Hysell and Burcham, 1998). Examples of these categories are presented in Fig. 2, which shows Bottom-type, Bottom-side, and Topside structures in panels (a) to (c), respectively. In general, from Fig. 2, the observed structures are visible mostly post-sunset and this coincides with the time when the generalized RTI is expected to intensify (Kelley, 2009). From panel (a) of Fig 2, Bottom-type structures are weak and narrow scattering layers and their thickness is less than about 50 km. Bottom-type layers do not cause strong ionogram spread F or intense radio scintillation at VHF frequencies and above. Their disturbance in the ionosphere is also not sufficient to cause signatures on air-glows (Hysell, 2000). Bottom-side structures correspond to broad, more structured, and stronger scattering layers at relatively higher altitudes that last for a few hours as seen in the middle panel of Fig 2, while Topside layers or radar plumes (see panel (c) of Fig. 2) represent larger-scale elongated structures originating from bottom-side layers and extending to the topside ionosphere (Hysell and Burcham, 1998; Hysell, 2000; Chapagain et al., 2009; Chapagain, 2011). They are indicators of strong plasma plumes (Smith et al., 2016).

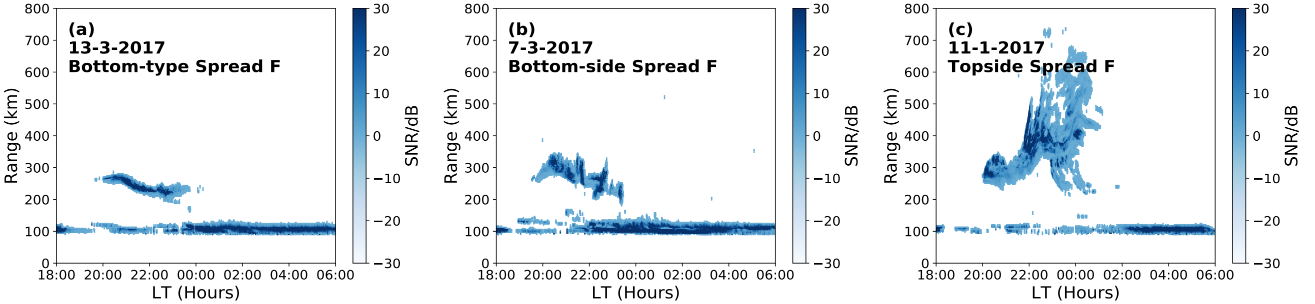

Figure 2. Examples of the different types of ESFs that may be observed by the JULIA radar. The color bar presents the signal to noise ratio (SNR) in dB.

To check the altitude coverage of the various types of plumes observed by the JULIA radar compared to the Swarm altitudes, a scatter plot of maximum heights was generated for the different types of plumes. To determine the plume maximum height, SNR outliers were first eliminated to minimize spurious data points. The maximum height then corresponds to the maximum range in km where SNR was recorded. Figure 3 shows a scatter plot of the maximum heights achieved by the various types of plumes for the years from 2014 to 2018 as a function of day of the month. From Fig. 3, the maximum heights of the

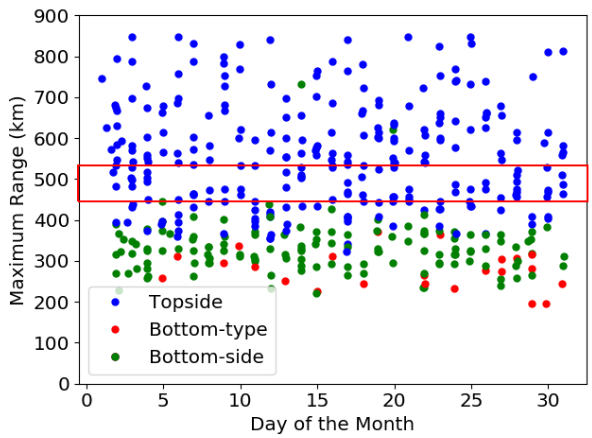

Figure 3. Maximum height achieved by the different types of ESFs observed by JULIA radar for the years from 2014 to 2018. The red rectangle indicates the approximate altitude coverage of the Swarm satellites from 2014 to 2018.

topside plasma plumes frequently coincide with the Swarm orbital altitudes. Therefore, Fig. 3 reveals that the Swarm orbits are strategically located and there is a high chance of Swarm to coincide with topside plasma structures compared to the other types. In this study, we considered topside plasma density structures for comparison with Swarm satellite N_e perturbation. The following subsection presents in situ observations of ionospheric irregularities by Swarm over or near the JRO longitude in comparison with the JULIA and ionosonde observations.

3.2 Coincident Ground-based and Swarm Observation of Ionospheric Irregularities

Here, in comparison with the ground-based observations, selected Swarm orbits that were directly overhead or passed close to the JRO are presented with observed plasma density structures. Figure 4 shows example cases on 2015-03-02 and 2015-03-08 where Swarm A and C passed directly over and near JRO, respectively. Column (i) of Fig. 4 shows the Range-Time-

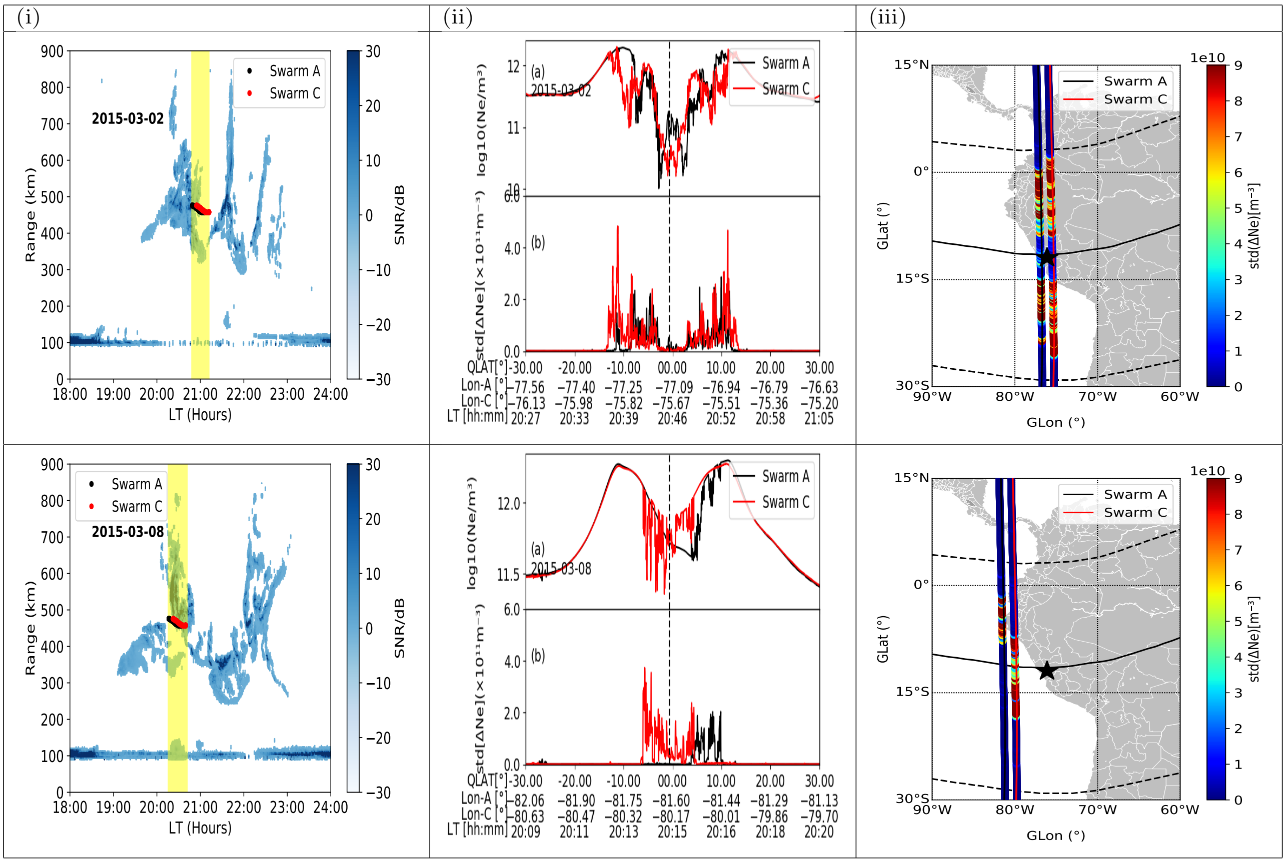

Figure 4. Examples of collocated observations by Swarm and JULIA radar on 2015-03-02 and 2015-03-08. The local time coverage and the corresponding altitude of Swarm while orbiting over or near JRO are (black for Swarm A, red for Swarm C) shaded yellow in column (i). The QLat of JRO is indicated with a vertical dotted black line in column (ii). The ground tracks of Swarm and the location of JRO are shown in the maps in column (iii). The thick black line in column (iii) shows the geomagnetic equator, while the dotted black lines show the EIA belts ($\pm 15^\circ$ QLat).

Intensity maps laid over with Swarm A and C positions. The JULIA radar started to detect weak 3-m irregularities from an altitude of about 300 km at about 1930 LT on 2015-03-02 and 2015-03-08. Gradually, the irregularities evolved into a series of spectacular plume structures that extended to altitudes of about 800 km. The plumes were only visible pre-midnight hours and this corresponds to the time when the RTI dominates (Kelley, 2009; Schunk and Nagy, 2009). The observed plasma plumes coincided with the Swarm passes.

Columns (ii) and (iii) of Fig. 4 show that Swarm encountered irregularity structures along their tracks for the case on 2015-03-02. The irregularities were more intense near the Equatorial Ionization Anomaly (EIA) belts at about $\pm 10^\circ - \pm 15^\circ$ QLat than at the quasi-dipole equator. Zakharenkova et al. (2016) analyzed one sample of plasma plumes recorded by JULIA and from the results they presented in Fig. 6, several Global Positioning System (GPS) satellites orbiting over the JRO encountered irregularities near the magnetic equator on 2015-03-02. Therefore, the structures observed by Swarm could be associated with the JULIA plasma plumes on 2015-03-02.

On 2015-03-08, Swarm A and C crossed the quasi-dipole equator in the evening sector at geographic longitudes of about 81.6°W and 80.17°W, respectively. The N_e profiles of Swarm A and C in columns (ii) and (iii) show depletions near the quasi-dipole equator. However, the longitudes of the Swarm satellites were offset from the JRO longitude to the west and ionospheric irregularities are generally assumed to drift westward across the magnetic field lines (Kelley, 2009). Burke et al. (2003) made a similar finding, comparing DMSP plasma density measurements with JULIA observations. Therefore, the depletions met by Swarm A and C may not correspond to the plumes observed by the JULIA radar. The irregularity structures observed by Swarm on 2015-03-08 may correspond to the plume remnants that drifted across the radar beam.

We also checked on the Spread F signatures on ionosonde data from JRO in comparison with the results presented in Fig. 4. Figures 5 and 6 show ionograms produced on 2015-03-02 and 2015-03-08 using the SAO explorer. The ionosonde measurements were recorded at 15 min intervals. The sequence of ionograms presented in Fig. 5 show that spread Fs were

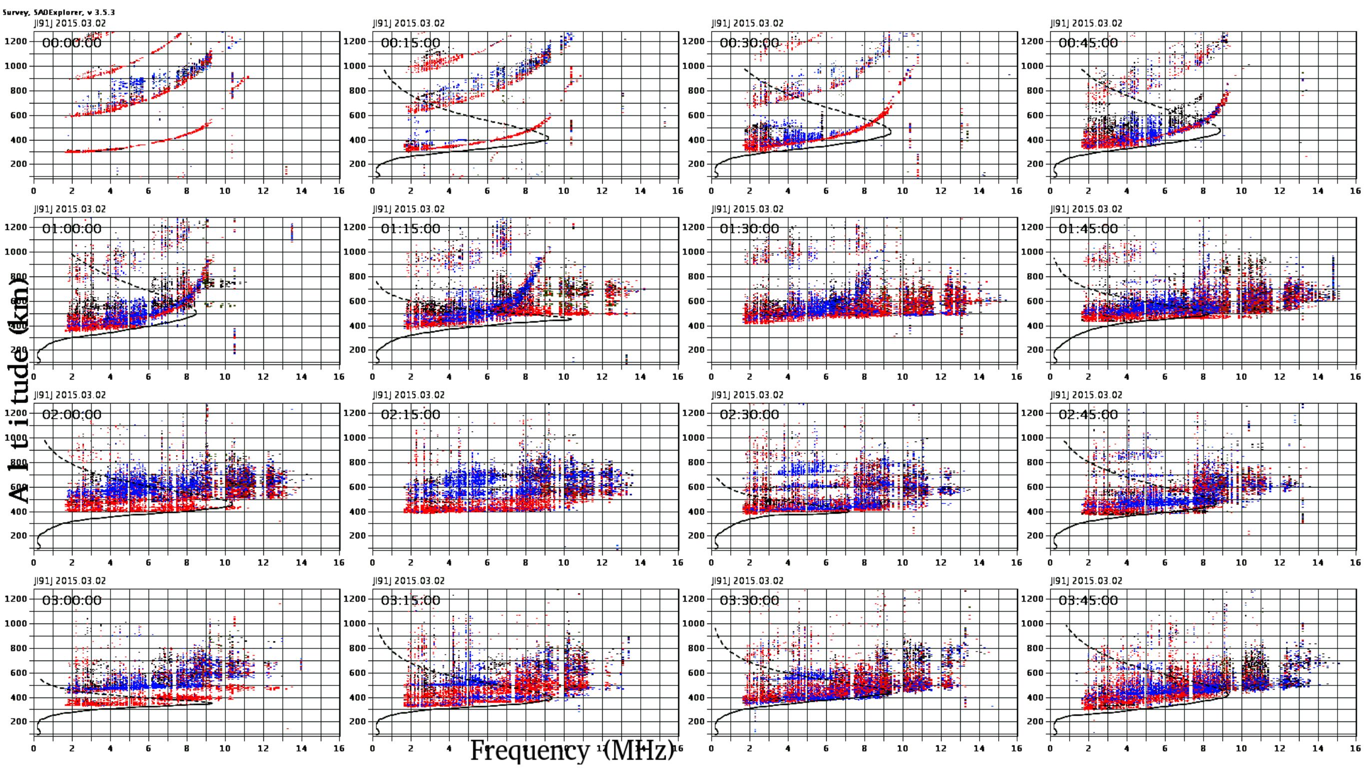

Figure 5. Ionograms showing occurrence of ESF on 2015-03-01 from 00:15 UT to 03:45 UT (LT= UT-5hrs).

continuously observed from 00:30 UT-05:00 UT (19:30 LT-24:00 LT), while Swarm encountered ionospheric irregularities on 2015-03-02 between about 20:27 LT to 21:05 LT (see Fig. 4). The ionograms on 2015-03-08 also showed strong spread Fs starting at 00:15 UT(19:15 LT) and this coincided with the time period when ionospheric irregularities and plasma plumes were recorded by Swarm and JULIA, respectively. The results presented in Fig. 4, 5, and 6 show that the in situ ionospheric irregularities, spread Fs, and plumes were observed over and near JRO simultaneously. Strong range spread F is caused by ionospheric irregularities and can, therefore, be regarded as a result of the generalized RTI mechanism (Rastogi et al., 1989; Wang et al., 2008; Shi et al., 2011; Alfonsi et al., 2013). The Spread F signatures are triggered by irregularities at the bottom or

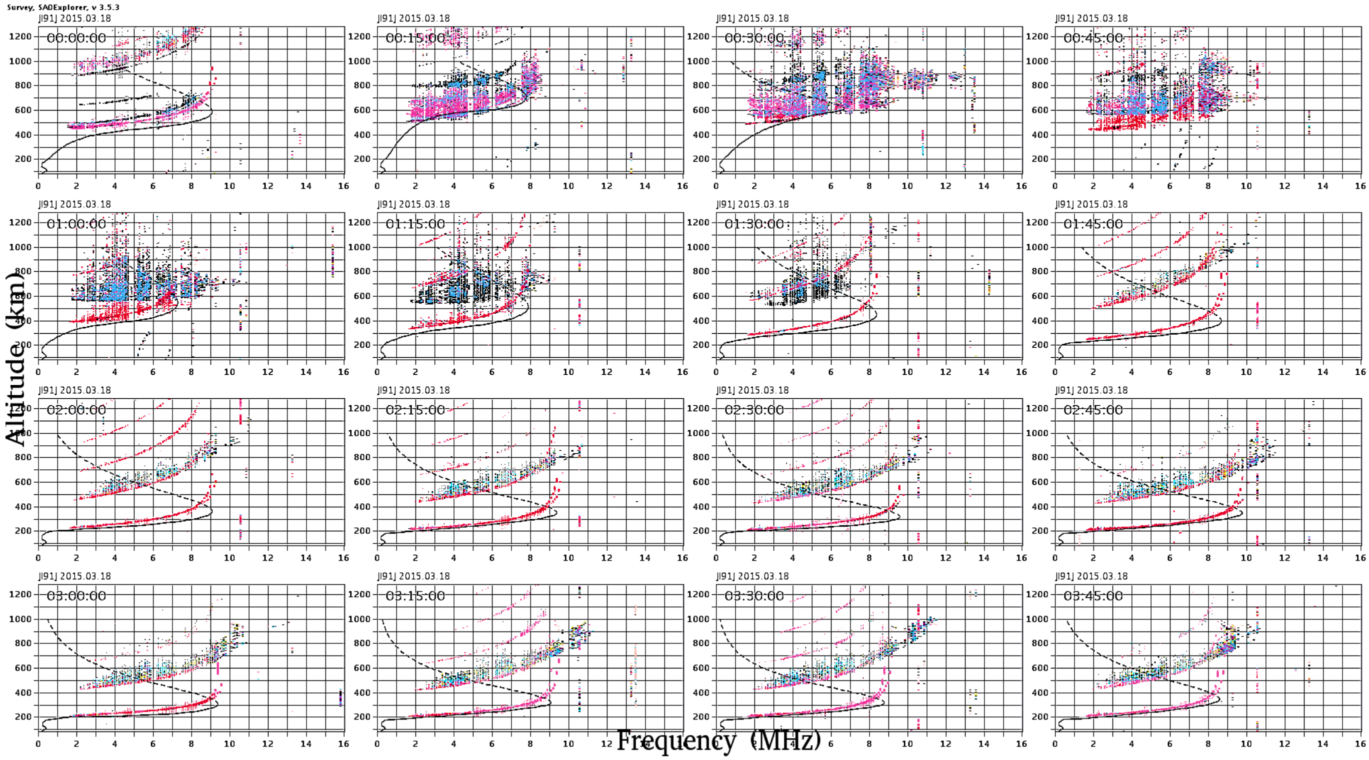

Figure 6. Ionograms showing occurrence of ESF on 2015-03-08 from 00:15 UT to 03:45 UT (LT= UT-5hrs).

within a growing plasma bubble or by declining bubbles (Abdu et al., 2012). Figures 4, 5, and 6 provide evidence that JULIA, Swarm, and ionosonde simultaneously observed ionospheric irregularities over the JRO. In the next section, we present the results of a statistical analysis of Swarm, JULIA, and ionosonde observations.

3.3 Statistical Analysis of Occurrence of Ionospheric Irregularities

The formation of equatorial ionospheric irregularities is influenced by several factors including local time, season, magnetic latitude and longitude. The data sets accumulated for the years from 2014 to 2018 were sufficient to compare the dependence of ground-based and in situ occurrence of ionospheric irregularities on various factors. Here, we present the results of statistical analysis carried out in this study. The specific details of each statistical result are described in the following subsections.

3.3.1 Statistics of Occurrence of Ionospheric Irregularities by Category

The Swarm satellites regress in longitude by about 22.5° between orbital ascending nodes. Therefore, in comparison with JULIA and ionosonde data, the Swarm passes were allowed to be within ±5° magnetic longitude of the JRO to make sure that a sufficient amount of Swarm passes could be used for the statistical examination. Summary plots such as those presented in Fig. 4 were generated for all days during the years from 2014 to 2018 for which the data was available. In total, 560 night-time orbits were used for which JULIA, Swarm, and ionosonde data were available concurrently. The outputs of the summary plots could be categorized into four cases considering the presence (or not) of irregularities. In general, these four cases are: Irregularities observed both on the ground and in situ, No irregularities observed both on the ground and in situ, Irregularities observed only in situ, and Irregularities observed only on the ground. For each RTI plot, the SNR corresponding to the peak height was determined and an event was identified as a significant irregularity when the peak height was $\geq$ 400 km. For peak height less than 400 km, these were classified as no irregularities. For the in situ Swarm observations, we considered a threshold of $1 \times 10^{10}\ \mathrm{m}^{-3}$ for std(ΔN_e) as a significant irregularity event, while for std(ΔN_e) less than the threshold were considered as no irregularities. For the ionosonde measurements, QF values greater than or equal to 20 km were considered as significant irregularity events. For each category, the percentage occurrence was computed as a ratio of the total number events in that category to the number of observations. These cases are presented in Fig. 7 for (a) Swarm and JULIA and (b) Swarm and ionosonde.

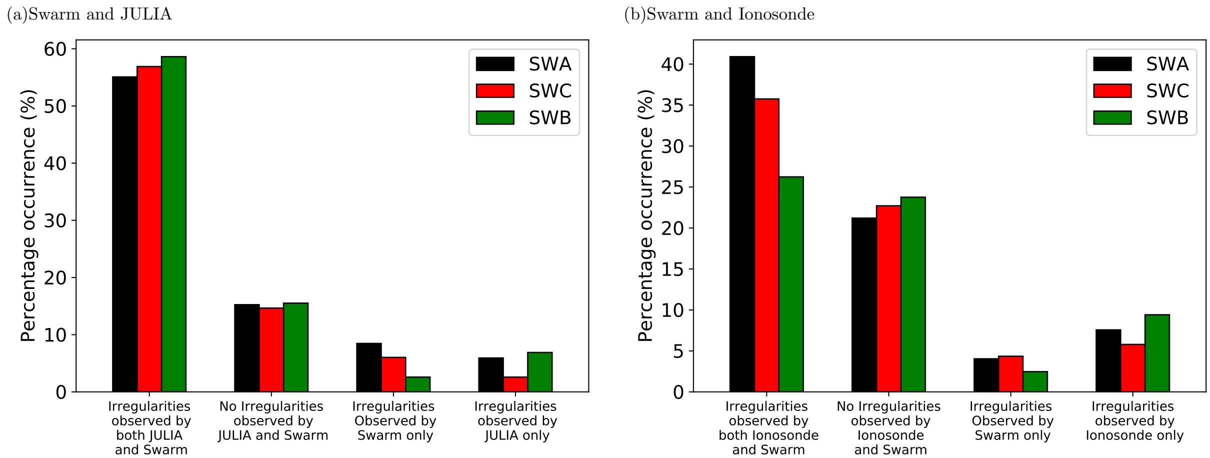

Figure 7. Percentage occurrence of irregularities in each category observed by the (a) Swarm satellites and JULIA observations and (b) Swarm satellites and ionosonde observations for the years from $2014 - 2018$.

In about 55.08% of the cases for Swarm A, 56.89% for Swarm C, and 58.62% of the cases for Swarm B, irregularity structures were detected by Swarm and JULIA as seen from panel (a) of Fig. 7. In about 15.25% of the cases for Swarm A, 14.66% for Swarm C, and 15.52% of the cases for Swarm B, no irregularity structures were detected by the Swarm satellites and JULIA. In panel (b) of Fig. 7, a high percentage occurrence was also observed when there was agreement (irregularities observed by both ionosonde and Swarm & no irregularities observed by ionosonde and Swarm) between Swarm and ionosonde. In general, the percentage occurrence was lower for ionosonde compared to JULIA and this may be due to low counting statistics. Nevertheless, the two categories where there was an agreement in panels (a) and (b) indicate that Swarm satellites, JULIA, and ionosonde simultaneously observed ionospheric irregularities. There were also some disagreements between the ground-based and space observations where JULIA and ionosonde detected plume structures, while Swarm registered no events as seen from the statistical results in panels (a) and (b) of Fig. 7. This suggests that plume structures may not have ascended to Swarm altitudes by the time the satellites passed over Jicamarca or the satellites were simply in a different location. For instances when Swarm registered events, while JULIA and ionosonde recorded no signatures, we checked on the longitudinal separation between the satellite passes and the ground-site. The longitudinal separations obtained between the Swarm passes and the ground site were often $\approx 5°$ and the magnitude of the in situ perturbations were relatively low. Ionospheric irregularities tend to be magnetic field aligned (Ossakow, 1979; Kil and Heelis, 1998; Nishioka et al., 2008; Kelley, 2009) and therefore, Swarm may encounter irregularities in situ of relatively small magnitudes, while JULIA and ionosonde do not identify any events, for wider longitudinal offset of a pass from the ground site.

In addition, for irregularities observed by Swarm only, Swarm B had the lowest percentage occurrence close to about 5% compared to Swarm A/C. The observed difference may be because of the progressive temporal and altitudinal separation between Swarm B and A/C (Zakharenkova et al., 2016). Swarm B orbits at a higher altitude compared to A/C and it crosses the same region later than A/C. Generally, in Fig. 7, a difference in percentage occurrence in all categories is observed between Swarm A and C although they orbit at the same altitude above sea-level. The large scale longitudinal bubble structure is sometimes observed with the two Swarm satellites (Xiong et al., 2016), but for small scale irregularities, the 1.5° longitudinal separation between the satellites is too large for a significant correlation between them.

3.3.2 Local time and Seasonal Variation of Ionospheric Irregularities

Numerous studies have shown that irregularity structures at low latitudes are a post-sunset phenomenon owing to the electrodynamics launched after sunset (e.g, Stolle et al., 2006; Lühr et al., 2014; Abdu et al., 2012). Here, we also compared the Local time dependence of occurrence of plasma plumes observed by the JULIA radar, spread-F recorded by the ionosonde, and small-scale ionospheric irregularities encountered by Swarm for different seasons. Figure 8 shows the percentage occurrence of plasma plumes as a function of local time and height grouped into different seasons i.e December solstice, June solstice, March equinox, and September Equinox. To obtain the results presented in Fig. 8, ground-based JULIA SNR data for the years from

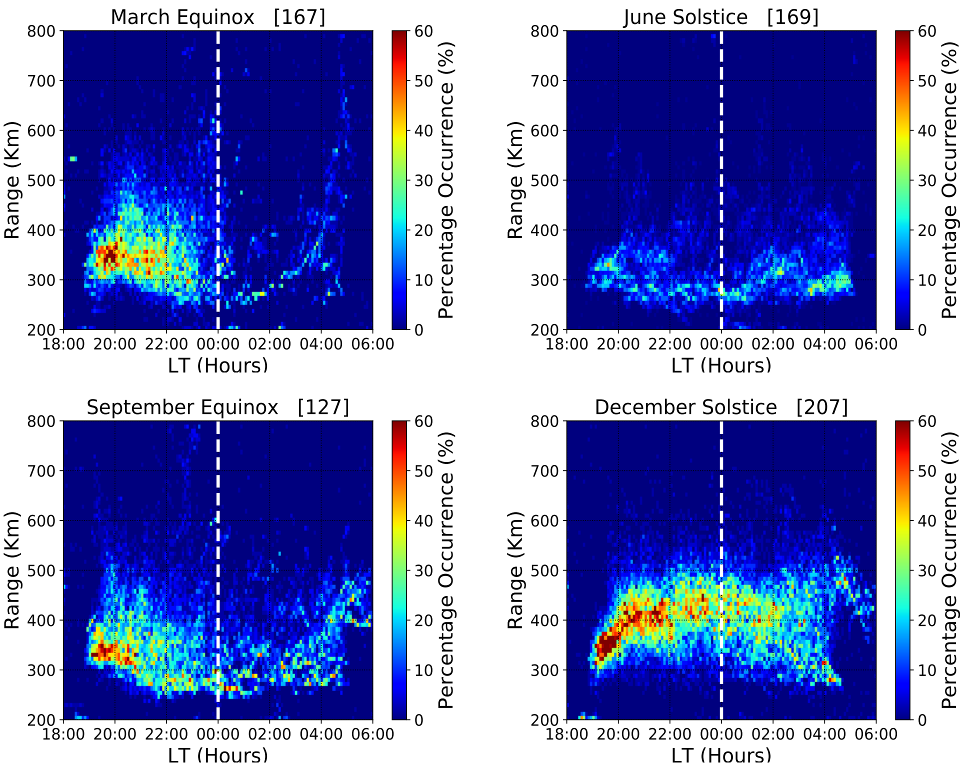

Figure 8. Percentage occurrence plasma plumes as a function of local time and height for the years $2014-2018$. Each panel represents a season. The number indicated in brackets is a count of days used to generate each season's statistics when measurements were made. The dotted white vertical line represents midnight.

2014 to 2018 were used. To eliminate the impact of geomagnetically disturbed conditions on the statistical outcomes, the data were filtered and only those recorded during quiet geomagnetic conditions ($\mathrm{Kp} \leq 3$) were taken into account. The JULIA data accumulated for the years from 2014 to 2018 were sufficient for examining the seasonal variation. Therefore, the seasonal dependence of local time distribution of JULIA observations of ionospheric irregularities was also examined by grouping all the data into different seasons corresponding to March Equinox (Feb-Mar-Apr), June Solstice (May-Jun-Jul), September Equinox (Aug-Sep-Oct), and December Solstice (Nov-Dec-Jan). For each local time-height bin, the percentage occurrence was obtained by dividing the number of observations with SNR > 10 dB by the total number of observations (e.g, Smith et al., 2016).

It is visible from Fig. 8 that the plasma plumes only occurred at night. Fig. 8 shows the occurrence of irregularities in plasma plumes starting at about 1900 LT and generally lasts past midnight. This observation is similar to the results presented in earlier studies (e.g, Kil and Heelis, 1998; Hysell and Burcham, 2002; Smith et al., 2016). The observed plasma plumes are connected with the nonlinear development of the RTI, which is initiated at the bottom of the F region. (Woodman and La Hoz, 1976; Huang, 2018). In December Solstice and the Equinoxes, the highest percentage occurrence occurs. The lowest percentage occurrence is observed in June Solstice. The daily variations of the vertical plasma drift measured by the ISR were used to better understand the seasonal patterns observed in Fig. 9. Figure 9 presents the Local time variation of F region vertical drift velocity for the years from 2014 to 2018. From Fig. 9, the PRE of the vertical plasma drifts can be seen around sunset hours

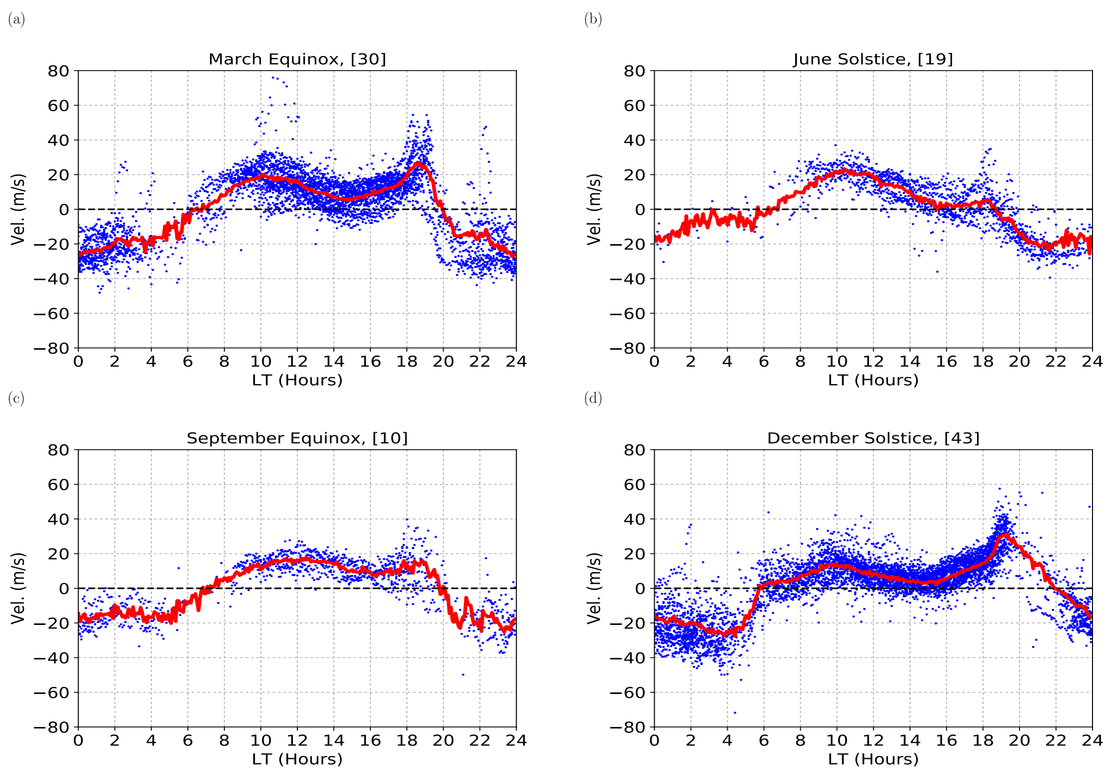

Figure 9. Local time variation of F- region vertical plasma drifts as a function of local time. The red curves represent the averaged vertical drift curves. Each panel represents a season.

(between 1700 LT and 2000 LT) before its reversal. Figure 9 shows the highest PRE peak in December Solstice and Equinox seasons, while the PRE peak is the lowest on June Solstice. Similar observations were made by Smith et al. (2016). Comparing the results presented in Fig. 9 with the local time distributions presented in Fig. 8, it follows that high occurrence of post-sunset topside spread F is associated with enhancements of the PRE peak. A high PRE implies significant $\boldsymbol{E} \times \boldsymbol{B}$ vertical drifts which boost the rate of RTI growth (Sultan, 1996; Fejer et al., 1999). The PRE pushes the ionospheric F layer to greater altitudes where collisions of ions with neutrals are less. The reduced collision causes the RTI to increase (Jayachandran et al., 1993; Kelley, 2009).

Figure 8 also shows a relatively high occurrence of irregularities after midnight especially in the solstices and September Equinox. Similar observations were made by Hysell and Burcham (2002) and Smith et al. (2016). The extension of the occurrence of plumes post-midnight may be due to the late reversal time and small post-reversal electric fields (Hysell and Burcham, 2002). Despite the use of transmitters of low power, the JULIA radar can also detect weak post-midnight irregularities, particularly during the solstice seasons as shown in Fig. 8. However, the detected post-midnight ionospheric irregularities often exist at much lower altitudes than the ones presented by Smith et al. (2016). Using Jicamarca radar measurements, Fejer et al. (1999) reported that the ionospheric irregularities that occur after midnight are typically well-formed structures that can be connected to the disturbed dynamo.

Figure 10 shows the QF indices derived from ionosonde observations as a function of local time and months. To obtain the results presented in Fig. 10, ground-based ionosonde data for the years from 2014 to 2018 were also used. The data were also filtered and only those recorded during quiet geomagnetic conditions were considered. To generate the results presented in Figure 10, for each month (y-axis), the QF indices were averaged over 1 hr Local time bins. Considering that equatorial

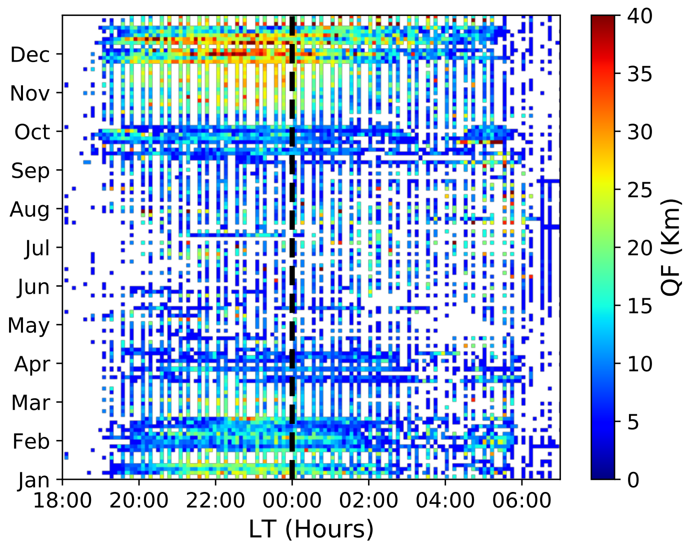

Figure 10. Month and local time (LT) variations of QF indices observed over JRO for the years from 2014-2018. The white spaces show periods when no spread F was detected. The dotted black vertical line represents midnight.

ionospheric irregularities are nighttime phenomena, we only presented QF data from 18:00 LT to 06:00 LT in Fig. 10. To generate Figure 10, for each month (y-axis), the QF were averaged over 0.1 hr Local time bins. Figure 10 shows that the QF index was high in the post-sunset period with peak values occurring between about 20:00 LT and 00:00 LT in December solstice and the equinoxes. The high QF values in the equinoxes and December solstice certainly is due to the RTI, which is usually triggered at the bottom side of a rising equatorial F layer. The rate of growth of the RTI depends on the meridional wind and the eastward electric field PRE determined by the longitudinal gradient of flux-tube-integrated conductivity (Sultan, 1996; Basu, 2002). In June solstice, QF values were small in the after sunset as seen in Fig. 10. Generally, Fig. 10 shows moderate QF values lasting till local midnight or longer (similar to the trend presented in Fig. 8). The low post-sunset QF values in June Solstice can be attributed to the small PRE and this can also be seen in panel (c) of Fig. 9.

Figure 11 shows the QLat-LT distributions of std(ΔN_e) for the Swarm satellites for the years from 2014 to 2018. Recall that the Swarm passes were allowed to be within $\pm 5^{\circ}$ magnetic longitude. The N_e data collected for the five years were

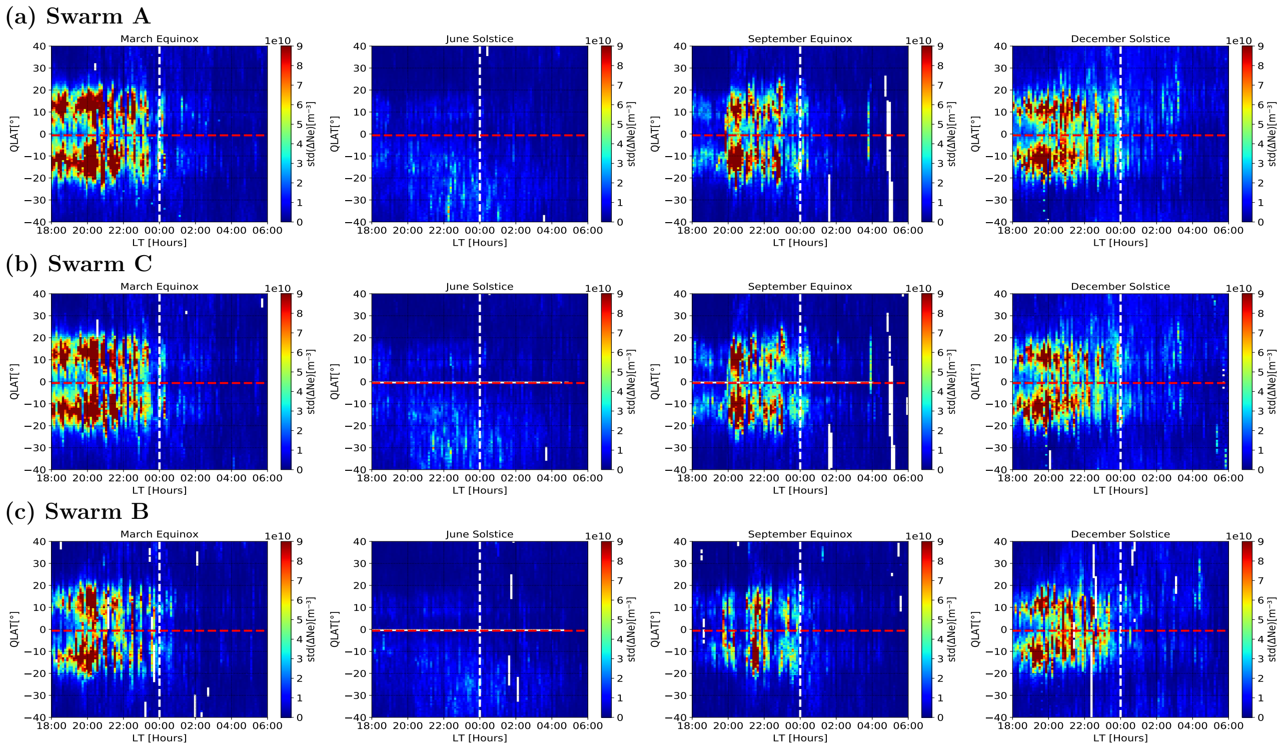

Figure 11. Quasi-dipole latitude and local time distributions of EPBs for Swarm A, C and B for the years from $2014-2018$. The dotted white vertical line represents midnight, while the dotted red horizontal line represents the quasi-dipole latitude of Jicamarca ($\approx -0.6°$). The white spaces represent data gaps.

also grouped into different seasons similar to those presented in Fig. 8. The results presented in Fig. 11 were also generated considering only the geomagnetically quiet conditions ($\mathrm{Kp} \leq 3$). The std(ΔN_e) was then calculated in bins of $1° \times 0.5$ hr resolution in QLat and Local time. The occurrence rate of ionospheric irregularities does not always correspond to the highest amplitude of irregularity structures (Wan et al., 2018). Therefore, we presented the calculated std(ΔN_e) per bin as a function of QLat and Local time as seen in Fig. 11. From Fig. 11, high std(ΔN_e) values frequently occurred between about $\pm 10° - \pm 20°$ QLat i.e., at the approximate location of the EIA belts. The distribution of the std(ΔN_e) as seen in Fig. 11 is essentially symmetrical about the quasi-dipole equator. The symmetrical distribution about the magnetic equator has also been observed in earlier studies (e.g, Stolle et al., 2006; Carter et al., 2013; Wan et al., 2018, etc) and this confirms that equatorial ionospheric irregularities usually extend along the magnetic field lines in the north and south directions and they are concentrated at the EIA belts (Kelley, 2009). The std(ΔN_e) attained a maximum between 20:00 LT and 22:00 LT. A decrease was detected after 22:00 LT until 06:00 LT. The local time distribution of std(ΔN_e) for Swarm A, B and C is the same as that of the quiet-time F-region echoes presented in Fig. 8 and the QF distribution presented in Fig. 10. The distribution of std(ΔN_e) shown in Fig. 11 has peak values at local times and QLat ranges where the RTI is expected. In terms of seasons, as observed from Fig. 11, high values of std(ΔN_e) were seen in the equinoxes and December solstice, while the lowest values were detected in June solstice. This is similar to the seasonal dependence of quiet-time F-region echoes presented in Fig. 8. From Fig. 11, Swarm hardly encountered post-midnight irregularities while orbiting over South America during all the seasons. From Fig. 8, it is

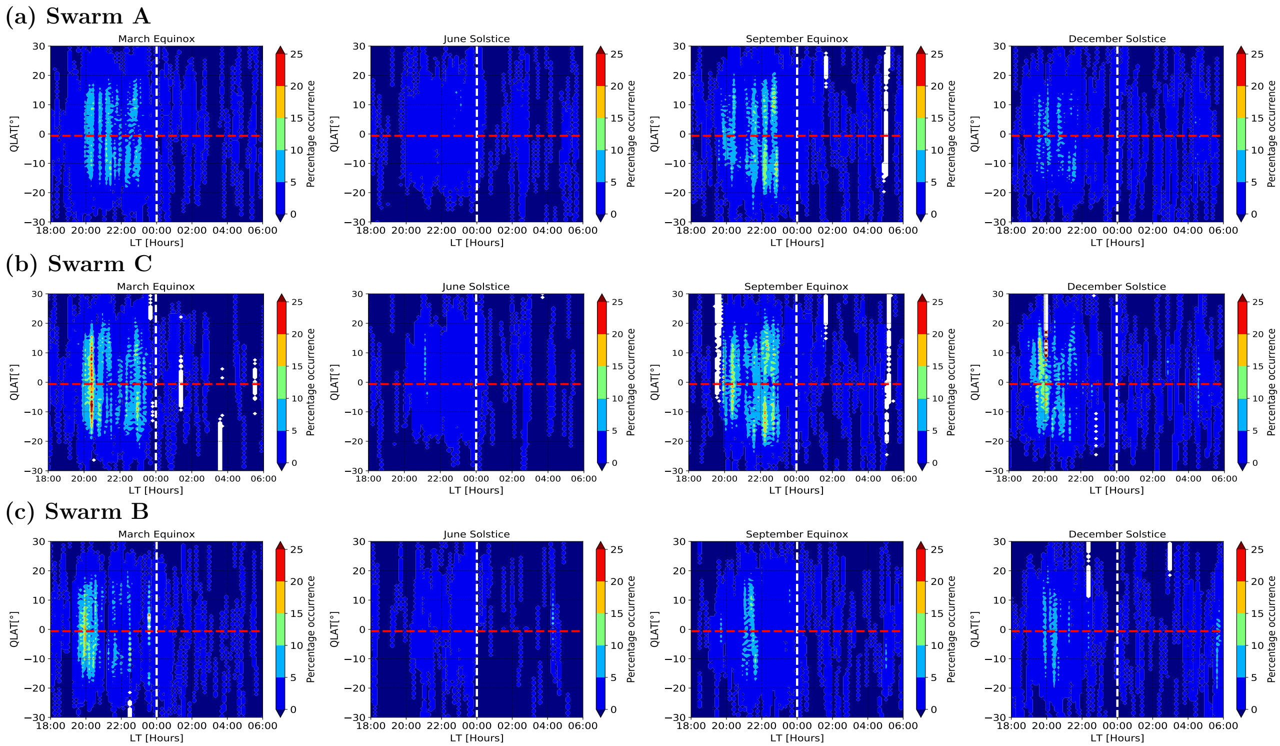

Figure 12. Quasi-dipole latitude and local time distributions of IBI for Swarm A, C and B for the years from $2014-2018$. The dotted white vertical line represents midnight, while the dotted red horizontal line represents the quasi-dipole latitude of Jicamarca ($\approx -0.6^{\circ}$). The white spaces represent data gaps.

observed that the post-midnight plumes often existed at lower altitudes in the solstices and September Equinox. Therefore, the low post-midnight ionospheric irregularity observations by Swarm may be because the plumes failed to reach Swarm altitudes.

For comparison, Fig. 12 shows the quasi-dipole versus local time distribution of ionospheric irregularities based on the IBI, which is a standard Level 2 product of the Swarm mission (Park et al., 2013). The IBI provides information on climatology of ionospheric irregularities and the level of magnetic field disturbance by taking both the electron density and magnetic field measurements into account (Park et al., 2013; Wan et al., 2018). It is important to note that the IBI is just either 1, 0, -1 for bubble detected, not detected or undetermined, respectively. Therefore, to generate the results in Fig. 12, the datasets were first grouped into different seasons corresponding to March Equinox (Feb-Mar-Apr), June Solstice (May-Jun-Jul), September Equinox (Aug-Sep-Oct), and December Solstice (Nov-Dec-Jan). For each season, the data was then binned into $1^{\circ} \times 0.1$ hr quasi-dipole latitude-local time bin. For each quasi-dipole latitude-local time bin, the percentage occurrence was obtained by dividing the number of observations with $\mathrm{IBI} = 1$ by the total number of observations. The binned percentage occurrence of $\mathrm{IBI} = 1$ shown in Fig. 12 shows similar results to the ones shown in Fig. 11, but with lower percentage occurrence. The low percentage occurrence of ionospheric irregularities derived from IBI was also observed by Wan et al. (2018). This may be because the magnitude of ionospheric irregularities must be large enough to cause magnetic field fluctuations Wan et al. (2018).

The Bragg condition for the JULIA radar implies that the coherent Spread echoes are from density variations at about 3 m wavelength (Kelley, 2009). The Bragg condition for backscatter means that a radar can only observe structures in the refractive index with size close to the half radar wavelength (Kelley, 2009; Hocking et al., 2016). The Swarm electron density measurements used in this study are limited by the sampling rate of 16 Hz and the orbital velocity of about 7.5 km/s to wavelengths of about 500 m, respectively, and longer. The good correlation between the Swarm measurements at these wavelengths and the Spread echoes from Swarm altitudes suggest that the irregularities seen by Swarm occur over a spectrum of different wavelengths, at least from about 500 m down to the radar wavelength of 3 m. A non-linear decay of unstable waves could explain this. In addition, we expect that the radar signal could be affected by scintillations which are particularly known from one-way signal propagation such as in GNSS and VHF satellite beacons (Burke et al., 2003; Zuo et al., 2016). For the radar, this could be relevant for echoes where the Bragg reflection occurs at high altitudes, above Swarm. Fresnel theory shows that wavelengths at the Fresnel scale of $\sqrt{(2\lambda d)}$ are most relevant for causing scintillations. λ is the wavelength, 3 m for the JULIA radar, and d the distance from the perturbation to the receiver, 445-510 km for Swarm. This gives a Fresnel scale between about 1.6 km and 1.7 km. The Swarm measurements generally indicate that irregularities at such scales are present near the paths of Bragg reflected radar signals. We, therefore, suggest that Spread F signals may at times be a result of both the Bragg backscattering at the highest altitude as well as scintillations of the radio waves to and from the scatter region.

4 Conclusions

In this paper, the results of a study of equatorial ionospheric irregularities detected by the JULIA radar and ionosonde in comparison with in situ N_e measurements made by Swarm for the years from 2014 to 2018 was presented. Cases of coincidence between Swarm, JULIA, and ionosonde observations were discussed. Also, the JULIA, ionosonde, and Swarm observations were examined statistically during geomagnetically quiet conditions. The local time and seasonal statistical patterns obtained from JULIA, ionosonde. and Swarm were explained using drift measurements by the ISR.

Results based on the JULIA radar and ionosonde agreed with the plasma density obtained from measurements of the Swarm faceplate for single satellite passes over or near the JRO. Basing on an on-off classification, in the majority of cases, when the JULIA radar detected topside plasma plumes, Swarm also observed plasma bubbles when its trajectory crossed directly overhead or near the JRO. This was also true for the ionosonde measurements. A few exceptions were also observed when the JULIA radar and ionosonde detected the presence of plasma structures, while Swarm did not record any bubbles and vice versa. For the case when JULIA and ionosonde recorded irregularity signatures, while Swarm observed no structures, the plume structures may not have ascended to Swarm altitudes by the time the satellites passed over Jicamarca or the satellites were simply in a different location. Swarm was able to detect ionospheric irregularities in situ, while no signature was recorded on the ground simply because the irregularities occurred at magnetic longitudes which were largely offset from the longitude of the ground-site. Statistical differences between Swarm A and C were observed and these were attributed to the 1.5° longitudinal separation between them which becomes significant for small scale irregularities.

The three phenomena i.e., plasma plumes observed by the JULIA radar, spread-Fs recorded by the ionosonde, and small scale irregularities detected by Swarm revealed similarities in the patterns of occurrence basing on local time and different seasons. The highest occurrence rate was observed on December Solstice and in the Equinoxes, while a low occurrence rate was observed on June Solstice. Measurements of the vertical plasma drift, made by the ISR, were used to understand the seasonal dependence of the occurrence of topside spread F and in situ density irregularities. The seasonal dependence of the occurrence of topside spread F and in situ N_e irregularities can be explained by the extent to which plasma is drifted vertically upwards.

The five years of Swarm faceplate N_e data set has revealed a lot of detailed features of electron density variations associated with plasma bubbles. In situ measurements of N_e by Swarm are a promising tool to indicate a likelihood of plasma plumes and spread F occurrence at times and locations where radar/ionosonde is not available. The geometry, however, is an important factor and therefore, in determining whether satellite observations are valid or accurate for any given ground site, algorithms should take into account the position of the satellite and the apex height of the magnetic field lines.

Data availability. The official website of Swarm is `http://earth.esa.int/swarm` and `ftp://swarm-diss.eo.esa.int` is the server for the distribution of Swarm data. The IBI measurements used in this study can be obtained from `https://swarm-diss.eo.esa.int/#swarm%2FLevel2daily%2FLatest_baselines%2FIBI`. The radar measurements used in this study can be obtained from the Madrigal database at `http://jro.igp.gob.pe/madrigal/`. The Kp index used in this study were obtained from the website `http://omniweb.gsfc.nasa.gov/`. The SAO Explorer software was obtained from `http://ulcar.uml.edu/SAO-X/SAO-X.html`.

Author contributions. The ideas presented in this manuscript were designed and implemented by Aol Sharon, Stephan Buchert, Edward Jurua, and Marco Milla. With contributions from all the co-authors, Aol Sharon prepared the manuscript.

Competing interests. The authors declare that there is no competing interest.

Acknowledgements. This study was financially supported by the International Science Program (ISP) of the Uppsala University, Sweden and by the Jicamarca International Research Experience Program (JIREP, `http://www.igp.gob.pe/convocatorias/jirep`) of the Instituto Geofisico del Peru with support from the US NSF. The authors acknowledge the ESA Swarm team for the Swarm mission. The Jicamarca Radio Observatory is a facility of the Instituto Geofisico del Peru operated with support from the NSF AGS-1732209 through Cornell University.

References

Aa, E., Zou, S., Ridley, A., Zhang, S., Coster, A. J., Erickson, P. J., Liu, S., and Ren, J.: Merging of Storm Time Midlatitude Traveling Ionospheric Disturbances and Equatorial Plasma Bubbles, Space Weather, 17, 285–298, https://doi.org/10.1029/2018sw002101, 2019.

Aa, E., Zou, S., Eastes, R., Karan, D. K., Zhang, S.-R., Erickson, P. J., and Coster, A. J.: Coordinated Ground-Based and Space-Based Observations of Equatorial Plasma Bubbles, Journal of Geophysical Research: Space Physics, 125, https://doi.org/10.1029/2019ja027569, 2020.

Abdu, M. A.: Outstanding problems in the equatorial ionosphere-thermosphere electrodynamics relevant to spread F, Journal of Atmospheric and Solar-Terrestrial Physics, 63, 869–884, https://doi.org/10.1016/S1364-6826(00)00201-7, 2001.

Abdu, M. A., Batista, I. S., Reinisch, B. W., MacDougall, J. W., Kherani, E. A., and Sobral, J. H. A.: Equatorial range spread F echoes from coherent backscatter, and irregularity growth processes, from conjugate point digital ionograms, Radio Science, 47, n/a–n/a, https://doi.org/10.1029/2012rs005002, 2012.

Alfonsi, L., Spogli, L., Pezzopane, M., Romano, V., Zuccheretti, E., Franceschi, G. D., Cabrera, M. A., and Ezquer, R. G.: Comparative analysis of spread-F signature and GPS scintillation occurrences at Tucumán, Argentina, Journal of Geophysical Research: Space Physics, 118, 4483–4502, https://doi.org/10.1002/jgra.50378, 2013.

Basu, B.: On the linear theory of equatorial plasma instability: Comparison of different descriptions, Journal of Geophysical Research (Space Physics), 107, 1199, https://doi.org/10.1029/2001JA000317, 2002.

Basu, S., McClure, J. P., Basu, S., Hanson, W. B., and Aarons, J.: Coordinated study of equatorial scintillation and in situ and radar observations of nighttime F region irregularities, Journal of Geophysical Research, 85, 5119–5130, https://doi.org/10.1029/JA085iA10p05119, 1980.

Booker, H. G. and Wells, H. W.: Scattering of radio waves by theF-region of the ionosphere, Journal of Geophysical Research, 43, 249, https://doi.org/10.1029/te043i003p00249, 1938.

Buchert, S.: Extended EFI LP data FP release notes, ESA Technical Note, 2016.

Burke, W. J., Huang, C. Y., Valladares, C. E., Machuzak, J. S., Gentile, L. C., and Sultan, P. J.: Multipoint observations of equatorial plasma bubbles, Journal of Geophysical Research (Space Physics), 108, 1221, https://doi.org/10.1029/2002JA009382, 2003.

Burke, W. J., Gentile, L. C., Huang, C. Y., Valladares, C. E., and Su, S. Y.: Longitudinal variability of equatorial plasma bubbles observed by DMSP and ROCSAT-1, Journal of Geophysical Research (Space Physics), 109, https://doi.org/10.1029/2004JA010583, 2004.

Carter, B. A., Zhang, K., Norman, R., Kumar, V. V., and Kumar, S.: On the occurrence of equatorial F-region irregularities during solar minimum using radio occultation measurements, Journal of Geophysical Research (Space Physics), 118, 892–904, https://doi.org/10.1002/jgra.50089, 2013.

Chapagain, N.: Dynamics of equatorial spread F using ground-based optical and radar measurements, 2011.

Chapagain, N. P., Fejer, B. G., and Chau, J. L.: Climatology of postsunset equatorial spread F over Jicamarca, Journal of Geophysical Research (Space Physics), 114, A07307, https://doi.org/10.1029/2008JA013911, 2009.

Cherniak, I., Zakharenkova, I., and Sokolovsky, S.: Multi-Instrumental Observation of Storm-Induced Ionospheric Plasma Bubbles at Equatorial and Middle Latitudes, Journal of Geophysical Research: Space Physics, 124, 1491–1508, https://doi.org/10.1029/2018ja026309, 2019.

Fejer, B. G., de Paula, E. R., Scherliess, L., and Batista, I. S.: Incoherent scatter radar, ionosonde, and satellite measurements of equatorialFregion vertical plasma drifts in the evening sector, Geophysical Research Letters, 23, 1733–1736, https://doi.org/10.1029/96gl01847, 1996.

Fejer, B. G., Scherliess, L., and de Paula, E. R.: Effects of the vertical plasma drift velocity on the generation and evolution of equatorial spreadF, Journal of Geophysical Research: Space Physics, 104, 19 859–19 869, https://doi.org/10.1029/1999ja900271, 1999.

Friis-Christensen, E., Lühr, H., and Hulot, G.: Swarm: A constellation to study the Earth's magnetic field, Earth, Planets, and Space, 58, 351–358, 2006.

Galkin, I. A., Khmyrov, G. M., Kozlov, A. V., Reinisch, B. W., Huang, X., Paznukhov, V. V., Song, P., Foster, J., Mendillo, M., and Bilitza, D.: The ARTIST 5, in: AIP Conference Proceedings, AIP, https://doi.org/10.1063/1.2885024, 2008.

Hickey, D. A., Martinis, C. R., Mendillo, M., Baumgardner, J., Wroten, J., and Milla, M.: Simultaneous 6300 Å airglow and radar observations of ionosphericirregularities and dynamics at the geomagnetic equator, Annales Geophysicae, 36, 473–487, https://doi.org/10.5194/angeo-36-473-2018, 2018.

Hocking, W. K., Röttger, J., Palmer, R. D., Sato, T., and Chilson, P. B.: Atmospheric radar: Application and science of MST radars in the Earth's mesosphere, stratosphere, troposphere, and weakly ionized regions, Cambridge University Press, 2016.

Huang, C.-S.: Effects of the postsunset vertical plasma drift on the generation of equatorial spread F, Progress in Earth and Planetary Science, 5, https://doi.org/10.1186/s40645-017-0155-4, 2018.

Huang, C.-S., La Beaujardiere, O., Roddy, P., Hunton, D., Liu, J., and Chen, S.: Occurrence probability and amplitude of equatorial ionospheric irregularities associated with plasma bubbles during low and moderate solar activities (2008–2012), Journal of Geophysical Research: Space Physics, 119, 1186–1199, https://doi.org/10.1002/2013ja019212, 2014.

Hysell, D. L.: An overview and synthesis of plasma irregularities in equatorial spread /F, Journal of Atmospheric and Solar-Terrestrial Physics, 62, 1037–1056, https://doi.org/10.1016/S1364-6826(00)00095-X, 2000.

Hysell, D. L. and Burcham, J. D.: JULIA radar studies of equatorial spread F, Journal of Geophysical Research, 103, 29 155–29 168, https://doi.org/10.1029/98JA02655, 1998.

Hysell, D. L. and Burcham, J. D.: Long term studies of equatorial spread /F using the JULIA radar at Jicamarca, Journal of Atmospheric and Solar-Terrestrial Physics, 64, 1531–1543, https://doi.org/10.1016/S1364-6826(02)00091-3, 2002.

Hysell, D. L., Larsen, M. F., and Woodman, R. F.: JULIA radar studies of electric fields in the equatorial electrojet, Geophysical Research Letters, 24, 1687–1690, https://doi.org/10.1029/97GL00373, 1997.

Hysell, D. L., Hedden, R. B., Chau, J. L., Galindo, F. R., Roddy, P. A., and Pfaff, R. F.: Comparing F region ionospheric irregularity observations from C/NOFS and Jicamarca, Journal of Geophysical Research, 36, L00C01, https://doi.org/10.1029/2009GL038983, 2009.

Jayachandran, B., Balan, N., Rao, P. B., Sastri, J. H., and Bailey, G. J.: HF Doppler and ionosonde observations on the onset conditions of equatorial spread F, Geophysical Research Letters, 98, 13, https://doi.org/10.1029/93JA00302, 1993.

Kelley, M.: The Earth's Ionosphere: Plasma Physics and Electrodynamics, International Geophysics, Elsevier Science, https://books.google.co.ug/books?id=3GlWQnjBQNgC, 2009.

Kelley, M. C., Rodrigues, F. S., Makela, J. J., Tsunoda, R., Roddy, P. A., Hunton, D. E., Retterer, J. M., de La Beaujardiere, O., de Paula, E. R., and Ilma, R. R.: C/NOFS and radar observations during a convective ionospheric storm event over South America, Geophysical Research Letters, 36, L00C07, https://doi.org/10.1029/2009GL039378, 2009.

Kil, H. and Heelis, R. A.: Global distribution of density irregularities in the equatorial ionosphere, Journal of Geophysical Research, 103, 407–418, https://doi.org/10.1029/97JA02698, 1998.

Kil, H., Paxton, L. J., and Oh, S.-J.: Global bubble distribution seen from ROCSAT-1 and its association with the evening prereversal enhancement, Journal of Geophysical Research: Space Physics, 114, n/a–n/a, https://doi.org/10.1029/2008ja013672, 2009.

Knudsen, D. J., Burchill, J. K., Buchert, S. C., Eriksson, A. I., Gill, R., Wahlund, J.-E., Åhlen, L., Smith, M., and Moffat, B.: Thermal ion imagers and Langmuir probes in the Swarm electric field instruments, Journal of Geophysical Research: Space Physics, https://doi.org/10.1002/2016ja022571, 2017.

Laundal, K. M. and Richmond, A. D.: Magnetic Coordinate Systems, Space Science Reviews, 206, 27–59, https://doi.org/10.1007/s11214-016-0275-y, 2016.

Lühr, H., Xiong, C., Park, J., and Rauberg, J.: Systematic study of intermediate-scale structures of equatorial plasma irregularities in the ionosphere based on CHAMP observations, Frontiers in Physics, 2, 15, https://doi.org/10.3389/fphy.2014.00015, 2014.

Ma, G. and Maruyama, T.: A super bubble detected by dense GPS network at east Asian longitudes, Geophysical Research Letters, 33, L21 103, https://doi.org/10.1029/2006GL027512, 2006.

Morse, F. A., Edgar, B. C., Koons, H. C., Rice, C. J., Heikkila, W. J., Hoffman, J. H., Tinsley, B. A., Winningham, J. D., Christensen, A. B., Woodman, R. F., Pomalaza, J., and Teixeira, N. R.: Equion, an equatorial ionospheric irregularity experiment, Journal of Geophysical Research, 82, 578–592, https://doi.org/10.1029/JA082i004p00578, 1977.

Ngwira, C. M., Klenzing, J., Olwendo, J., D'ujanga, F. M., Stoneback, R., and Baki, P.: A study of intense ionospheric scintillation observed during a quiet day in the East African low-latitude region, Radio Science, 48, 396–405, https://doi.org/10.1002/rds.20045, 2013a.

Ngwira, C. M., Seemala, G. K., and Bosco Habarulema, J.: Simultaneous observations of ionospheric irregularities in the African low-latitude region, Journal of Atmospheric and Solar-Terrestrial Physics, 97, 50–57, https://doi.org/10.1016/j.jastp.2013.02.014, 2013b.

Nishioka, M., Saito, A., and Tsugawa, T.: Occurrence characteristics of plasma bubble derived from global ground-based GPS receiver networks, Journal of Geophysical Research: Space Physics, 113, https://doi.org/10.1029/2007ja012605, 2008.

Nishioka, M., Basu, S., Basu, S., Valladares, C. E., Sheehan, R. E., Roddy, P. A., and Groves, K. M.: C/NOFS satellite observations of equatorial ionospheric plasma structures supported by multiple ground-based diagnostics in October 2008, Journal of Geophysical Research: Space Physics, 116, n/a–n/a, https://doi.org/10.1029/2011ja016446, 2011.

Ossakow, S. L.: Ionospheric irregularities, Reviews of Geophysics, 17, 521–533, https://doi.org/10.1029/RG017i004p00521, 1979.

Otsuka, Y., Shiokawa, K., Ogawa, T., Yokoyama, T., Yamamoto, M., and Fukao, S.: Spatial relationship of equatorial plasma bubbles and field-aligned irregularities observed with an all-sky airglow imager and the Equatorial Atmosphere Radar, Geophysical Research Letters, 31, L20802, https://doi.org/10.1029/2004GL020869, 2004.

Park, J., Noja, M., Stolle, C., and Lühr, H.: The Ionospheric Bubble Index deduced from magnetic field and plasma observations onboard Swarm, Earth, Planets and Space, 65, 1333–1344, https://doi.org/10.5047/eps.2013.08.005, 2013.

Rastogi, R. G., Koparkar, P. V., Chandra, H., and Vyas, G. D.: Spread-F and radio wave scintillations near the F-region anomaly crest, Annales Geophysicae, 7, 281–284, 1989.

Reinisch, B., Huang, X., Galkin, I., Paznukhov, V., and Kozlov, A.: Recent advances in real-time analysis of ionograms and ionospheric drift measurements with digisondes, Journal of Atmospheric and Solar-Terrestrial Physics, 67, 1054–1062, https://doi.org/10.1016/j.jastp.2005.01.009, 2005.

Reinisch, B. W., Scali, J. L., and Haines, D. L.: Ionospheric drift measurements with ionosondes, Annals of Geophysics, 41, https://doi.org/10.4401/ag-3812, 1998.

Roddy, P. A., Hunton, D. E., Ballenthin, J. O., and Groves, K. M.: Correlation of in situ measurements of plasma irregularities with ground-based scintillation observations, Journal of Geophysical Research (Space Physics), 115, A06303, https://doi.org/10.1029/2010JA015288, 2010.

Schunk, R. W. and Nagy, A. F.: Ionospheres: physics, plasma physics, and chemistry, Cambridge Atmospheric and Space Science Series, Cambridge, Cambridge, 2 edn., 2009.

Shi, J. K., Wang, G. J., Reinisch, B. W., Shang, S. P., Wang, X., Zherebotsov, G., and Potekhin, A.: Relationship between strong range spreadFand ionospheric scintillations observed in Hainan from 2003 to 2007, Journal of Geophysical Research: Space Physics, 116, A08 306, https://doi.org/10.1029/2011ja016806, 2011.

Siefring, C. L., Bernhardt, P. A., Roddy, P. A., and Hunton, D. E.: Comparisons of equatorial irregularities measurements from C/NOFS: TEC using CERTO and CITRIS with in-situ plasma density, Geophysical Research Letters, 36, L00C08, https://doi.org/10.1029/2009GL038985, 2009.

Smith, J. M., Rodrigues, F. S., and de Paula, E. R.: Radar and satellite investigations of equatorial evening vertical drifts and spread F, Annales Geophysicae, 33, 1403–1412, https://doi.org/10.5194/angeo-33-1403-2015, 2015.

Smith, J. M., Rodrigues, F. S., Fejer, B. G., and Milla, M. A.: Coherent and incoherent scatter radar study of the climatology and day-to-day variability of mean F region vertical drifts and equatorial spread F, Journal of Geophysical Research (Space Physics), 121, 1466–1482, https://doi.org/10.1002/2015JA021934, 2016.

Sripathi, S., Bose, S., Patra, A. K., Pant, T. K., Kakad, B., and Bhattacharyya, A.: Simultaneous observations of ESF irregularities over Indian region using radar and GPS, Annales Geophysicae, 26, 3197–3213, https://doi.org/10.5194/angeo-26-3197-2008, 2008.

Stolle, C., Lühr, H., Rother, M., and Balasis, G.: Magnetic signatures of equatorial spread F as observed by the CHAMP satellite, Journal of Geophysical Research (Space Physics), 111, A02304, https://doi.org/10.1029/2005JA011184, 2006.

Sultan, P. J.: Linear theory and modeling of the Rayleigh-Taylor instability leading to the occurrence of equatorial spread F, Journal of Geophysical Research, 101, 26 875–26 892, https://doi.org/10.1029/96JA00682, 1996.

Tsunoda, R. T.: On the spatial relationship of 1-m equatorial spread F-irregularities and plasma bubbles, Journal of Geophysical Research, 85, 185–190, https://doi.org/10.1029/JA085iA01p00185, 1980.

Tsunoda, R. T., Livingston, R. C., McClure, J. P., and Hanson, W. B.: Equatorial plasma bubbles - Vertically elongated wedges from the bottomside F layer, Journal of Geophysical Research, 87, 9171–9180, https://doi.org/10.1029/JA087iA11p09171, 1982.

Wan, X., Xiong, C., Rodriguez-Zuluaga, J., Kervalishvili, G. N., Stolle, C., and Wang, H.: Climatology of the Occurrence Rate and Amplitudes of Local Time Distinguished Equatorial Plasma Depletions Observed by Swarm Satellite, Journal of Geophysical Research, Space Physics, 123, 3014–3026, https://doi.org/10.1002/2017JA025072, 2018.

Wang, G., Shi, J., Wang, X., and Shang, S.: Seasonal variation of spread-F observed in Hainan, Advances in Space Research, 41, 639–644, https://doi.org/10.1016/j.asr.2007.04.077, 2008.

Wang, G. J., Shi, J. K., Reinisch, B. W., Wang, X., and Wang, Z.: Ionospheric plasma bubbles observed concurrently by multi-instruments over low-latitude station Hainan, Journal of Geophysical Research: Space Physics, 120, 2288–2298, https://doi.org/10.1002/2014JA020245, 2015.

Wang, Z., Shi, J. K., Torkar, K., Wang, G. J., and Wang, X.: Correlation between ionospheric strong range spread F and scintillations observed in Vanimo station, Journal of Geophysical Research: Space Physics, 119, 8578–8585, https://doi.org/10.1002/2014ja020447, 2014.

Woodman, R. F. and La Hoz, C.: Radar observations of F region equatorial irregularities, Journal of Geophysical Research, 81, 5447–5466, https://doi.org/10.1029/JA081i031p05447, 1976.

Xiong, C., Stolle, C., Juan, R. Z., and Siemes, C.: Losses of GPS signals onboard the Swarm satellites and its relation to strong plasma depletions, AGU Fall Meeting Abstracts, pp. SA12A–01, 2016.

Yeh, K. C. and Liu, C.-H.: Radio wave scintillations in the ionosphere, IEEE Proceedings, 70, 324–360, https://doi.org/10.1109/proc.1982.12313, 1982.

Zakharenkova, I., Astafyeva, E., and Cherniak, I.: GPS and in situ Swarm observations of the equatorial plasma density irregularities in the topside ionosphere, Earth, Planets, and Space, 68, 120, https://doi.org/10.1186/s40623-016-0490-5, 2016.

Zhan, W., Rodrigues, F. S., and Milla, M. A.: On the Genesis of Postmidnight Equatorial Spread F : Results for the American/Peruvian Sector, Geophysical Research Letters, 45, 7354–7361, https://doi.org/10.1029/2018gl078822, 2018.

Zhang, Y., Wan, W., Li, G., Liu, L., Hu, L., and Ning, B.: A comparative study of GPS ionospheric scintillations and ionogram spread F over Sanya, Annales Geophysicae, 33, 1421–1430, https://doi.org/10.5194/angeo-33-1421-2015, 2015.

Zuo, X., Yu, T., and Xia, C.: A study of simultaneous scintillation observations by Chinese FY-2 geostationary meteorological satellite and VHF coherent radar measurements over South China, AGU Fall Meeting Abstracts, SA13A-2111, 2016.